ResearchGate

See discussions, stats, and author profiles for this publication at: https://www.researchgate.net/publication/8265259

Expression and Characterization of the Two Flavodoxin Proteins of Bacillus subtilis , YkuN and YkuP: Biophysical Properties and Interactions with Cytochrome P450 BioI †

ARTICLE *in* BIOCHEMISTRY · OCTOBER 2004

Impact Factor: 3.02 · DOI: 10.1021/bi049131t · Source: PubMed

CITATIONS
49

READS
14

5 AUTHORS, INCLUDING:

Claes von Wachenfeldt
Lund University
38 PUBLICATIONS **1,360** CITATIONS
SEE PROFILE

John B Perkins
Royal DSM
32 PUBLICATIONS **1,846** CITATIONS
SEE PROFILE

Andrew W Munro
The University of Manchester
206 PUBLICATIONS **5,368** CITATIONS
SEE PROFILE

Available from: John B Perkins
Retrieved on: 24 January 2016

Expression and Characterization of the Two Flavodoxin Proteins of *Bacillus subtilis*, YkuN and YkuP: Biophysical Properties and Interactions with Cytochrome P450 BioI†

Rachel J. Lawson,‡ Claes von Wachenfeldt,§ Ihtshamul Haq,⊥ John Perkins,|| and Andrew W. Munro*,‡

Department of Biochemistry, University of Leicester, The Adrian Building, University Road, Leicester LE1 7RH, U.K., Department of Cell and Organism Biology, Lund University, Sölvegatan 35, SE-223 62 Lund, Sweden, Centre for Chemical Biology, Department of Chemistry, University of Sheffield, Brook Hill, Sheffield, S3 7HK, U.K., and Biotechnology Research and Development, DSM Nutritional Products, P.O. Box 3255, Building 203/20A, CH-4002, Basel, Switzerland

Received April 29, 2004; Revised Manuscript Received July 23, 2004

ABSTRACT: The two flavodoxins (YkuN and YkuP) from *Bacillus subtilis* have been cloned, overexpressed in *Escherichia coli* and purified. DNA sequencing, mass spectrometry, and flavin-binding properties showed that both YkuN and YkuP were typical short-chain flavodoxins (158 and 151 amino acids, respectively) and that an error in the published *B. subtilis* genome sequence had resulted in an altered reading frame and misassignment of YkuP as a long-chain flavodoxin. YkuN and YkuP were expressed in their blue (neutral semiquinone) forms and reoxidized to the quinone form during purification. Potentiometry confirmed the strong stabilization of the semiquinone form by both YkuN and YkuP (midpoint reduction potential for oxidized/semiquinone couple = −105 mV/−105 mV) with respect to the hydroquinone (midpoint reduction potential for semiquinone/hydroquinone couple = −382 mV/−377 mV). Apoflavodoxin forms were generated by trichloroacetic acid treatment. Circular dichroism studies indicated that flavin mononucleotide (FMN) binding led to considerable structural rearrangement for YkuP but not for YkuN. Both apoflavodoxins bound FMN but not riboflavin avidly, as expected for short-chain flavodoxins. Structural stability studies with the chaotrope guanidinium chloride revealed that there is moderate destabilization of secondary and tertiary structure on FMN removal from YkuN, but that YkuP apoflavodoxin has similar (or slightly higher) stability compared to the holoprotein. Differential scanning calorimetry reveals further differences in structural stability. YkuP has a lower melting temperature than YkuN, and its endotherm is composed of a single transition, while that for YkuN is biphasic. Optical and fluorimetric titrations with oxidized flavodoxins revealed strong affinity (K_d values consistently <5 μM) for their potential redox partner P450 BioI, YkuN showing tighter binding. Stopped-flow reduction studies indicated that the maximal electron-transfer rate (k_{red}) to fatty acid-bound P450 BioI occurs from YkuN and YkuP at $\sim$2.5 s^{-1}, considerably faster than from *E. coli* flavodoxin. Steady-state turnover with YkuN or YkuP, fatty acid-bound P450 BioI, and *E. coli* NADPH−flavodoxin reductase indicated that both flavodoxins supported lipid hydroxylation by P450 BioI with turnover rates of up to $\sim$100 min^{-1} with lauric acid as substrate. Interprotein electron transfer is a likely rate-limiting step. YkuN and YkuP supported monohydroxylation of lauric acid and myristic acid, but secondary oxygenation of the primary product was observed with both palmitic acid and palmitoleic acid as substrates.

The cytochromes P450 (P450s) are heme *b*-containing monooxygenases that participate in a plethora of physiologically important reactions (*1*). Typical P450s require donation of two electrons from a redox partner enzyme(s) to generate a reactive ferryl−oxygen intermediate that appears to be the major oxidant in P450-mediated reactions (*2*, *3*). For virtually all P450 systems, specific redox systems (usually flavin, iron−sulfur center-containing proteins, or both) are required for the electron transport process in vivo. The best-studied P450 redox systems are the so-called "class 1" and "class 2" electron-transfer partners. Class 1 are NAD(P)H−ferredoxin reductase and iron−sulfur ferredoxin proteins, typified by putidaredoxin reductase and putidaredoxin in the P450 cam camphor hydroxylase system from *Pseudomonas putida* (*4*, *5*). Class 2 are represented by the membranous NADPH-dependent diflavin (flavin adenine dinucleotide (FAD)- and flavin mononucleotide (FMN)-containing) enzyme cytochrome P450 reductase (CPR)[1] found in eukaryotic microsomal P450 systems (*6*, *7*). These systems have been inten-

† These studies were funded by the Biotechnology and Biological Sciences Research Council (BBSRC, U.K.) and through a BBSRC studentship award to R.J.L. co-funded by DSM Nutritional Products.

* Author for correspondence: phone 0044 116 252 3454, fax 0044 116 252 3369, e-mail awm9@le.ac.uk.

‡ University of Leicester.

§ Lund University.

⊥ University of Sheffield.

|| DSM Nutritional Products.

[1] Abbreviations: BioI, cytochrome P450 BioI from *Bacillus subtilis*; CPR, cytochrome P450 reductase; DSC, differential scanning calorimetry; DTT, dithiothreitol; Fer, Fe_4S_4 ferredoxin from *Bacillus subtilis*; FLDR, *E. coli* flavodoxin reductase; GdmCl, guanidinium chloride; NOS, nitric oxide synthase; T_m, melting temperature.

10.1021/bi049131t CCC: $27.50 © 2004 American Chemical Society
Published on Web 09/04/2004

sively studied, and a wealth of kinetic, spectroscopic, and structural data is available (e.g., refs *8* and *9*). The discovery of the fusion protein flavocytochrome P450 BM3 from *Bacillus megaterium* provided the first clear evidence that nature might operate different types of redox apparatus to drive P450-mediated reactions (*10*). P450 BM3 is a fatty acid hydroxylase in which a soluble CPR (devoid of an N-terminal membrane anchor region found in eukaryotic CPRs) is fused to a soluble P450, forming a highly efficient electron-transfer chain (*11*, *12*). Subsequent studies have confirmed the diversity of microbial P450 reductase apparatus, revealing such systems as P450s that interact directly with NADH (the nitric oxide reductase P450 nor from *Fusarium oxysporum*, ref *13*) or peroxide (the fatty acid-binding P450 BSβ from *B. subtilis*, ref *14*) or in which P450s are fused to a phthalate dioxygenase reductase-like electron-transfer module (*15*).

In the *B. subtilis* P450 BioI system (see ref *36*), a gene encoding an Fe_4S_4 protein (*fer*) is located distant from the *bioI* gene on the chromosome. Fer is the only low molecular weight ferredoxin apparent on the *B. subtilis* chromosome (*16*). The ferredoxin has been expressed and characterized and shown to support electron transfer to BioI (*17*). Previous work on P450 systems has demonstrated that Fe_2S_2 and Fe_3S_4 cluster-containing ferredoxins are the native redox partners supporting the function of P450s from both eukaryotic and prokaryotic P450 enzymes (*18*, *19*). However, should Fer be the natural redox partner for BioI, it would be the first Fe_4S_4 cluster ferredoxin assigned such a function. Fer is the sole ferredoxin in the *B. subtilis* genome, so there are no alternatives should ferredoxin-supported catalysis prove to be the case for P450 BioI (*20*). In this respect, it is notable that a bacterial flavodoxin (cindoxin from *Citrobacter braakii*) has been reported to mediate electron transfer to BioI and to support its oxidative function (*21*, *22*). This flavodoxin has also been reported as the natural redox partner for $P450_{cin}$ (CYP176A), a cineole-degrading P450, providing evidence that flavodoxins are physiologically relevant redox partners of bacterial P450s (*23*). Also, the FMN-containing domain of CPR is evolutionarily related to flavodoxins (*24*). *B. subtilis* encodes two putative flavodoxins (encoded by the *ykuN* and *ykuP* genes, located at 1486.3 kb and 1487.7 kb on the chromosome, respectively). Potentially, one (or both) of these predicted flavoproteins are the natural redox partners for P450 BioI, supporting its critical function in the synthesis of the vitamin biotin.

Flavodoxins are small (typically 14−23 kDa) FMN-binding proteins found in a wide range of microbes, including aerobic and anaerobic bacteria, algae, and other lower eukaryotes (*25*). They act as single electron carriers between other redox proteins, and most flavodoxin-dependent redox reactions are considered to occur with the flavodoxin cycling between its hydroquinone and semiquinone forms. However, there is evidence for the involvement of flavodoxin semiquinone as the electron donor in the reaction of *Escherichia coli* methionine synthase (*26*). Aside from this important reaction, flavodoxins are also known to be critical to, for example, nitrogen fixation reactions in *Klebsiella pneumoniae* (*27*), the reductive activation of pyruvate-formate lyase in *E. coli* (*28*), and the reductive activation of biotin synthase, the final enzymatic step in the synthesis of biotin (*29*). While their biosynthesis is constitutive in *E. coli* and certain other bacteria, flavodoxin production in many microbes is up-regulated under low iron conditions. Thus, they may surrogate for ferredoxin(s) in various physiological roles (*25*). The flavodoxins are structurally well-characterized and share a common fold in which a central β sheet region is flanked on both sides by α helices (*30*). FMN cofactor is tightly but noncovalently bound and partly solvent-exposed. Single flavodoxins have been reported in several bacteria, but *E. coli* contains two (FldA and FldB), and the genome sequence of *B. subtilis* indicates that two flavodoxins are also present in this organism and are closely linked on the chromosome (*20*). The putative flavodoxins (*ykuN* and *ykuP*) are separated only by the *ykuO* gene, which encodes a protein of unknown function. It appears that *ykuN*, *ykuO*, and *ykuP* are organized in an operon (Figure 1); σ^A-type promoters, which are recognized by the principal σ factor of the cell, can be identified upstream of *ykuN* and just downstream of *ykuP* (that is, in front of the *ykuQ* gene). The *ykuNOP* operon is part of the *fur* regulon (*31*). The ferric uptake repressor (Fur) regulates expression in response to iron starvation, suggesting that the YkuN and YkuP proteins may be expressed under conditions in which the production of the sole ferredoxin (Fer) of *B. subtilis* is diminished (*17*). Involvement of flavodoxin in the synthesis of biotin is already established. At the final, rate-limiting stage in the reaction scheme (the generation of biotin from dethiobiotin), *E. coli* flavodoxin (FldA) and its redox partner NADPH−flavodoxin reductase (FLDR) provide electrons for the reaction catalyzed by biotin synthase (*32*, *33*). On the basis of studies with the flavodoxin cindoxin from *C. brakii* (*21*), it appears likely that flavodoxin is also involved at the earlier stage of the *B. subtilis* biotin synthesis pathway involving P450 BioI.

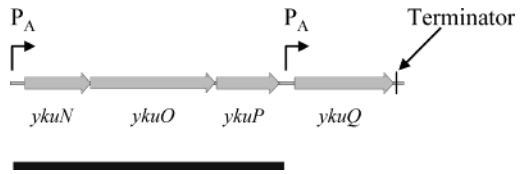

FIGURE 1: Genomic organization of *ykuN* and *ykuP*. The *ykuN*, *ykuO*, and *ykuP* genes are proposed to be cotranscribed from a σ^A-type promoter (indicated by an arrow and the symbol "P_A"). The *ykuN*−*Q* genes are indicated by gray, filled arrows. The predicted mRNA containing *ykuNOP* is indicated as a thick black line. A further σ^A-type promoter is located just downstream of *ykuP* and is predicted to control transcription of the *ykuQ* gene. A transcriptional terminator is evident immediately following the *ykuQ* gene.

In this manuscript, we report the cloning, expression, purification, and characterization of the YkuN and YkuP proteins of *B. subtilis*. They are both shown to be FMN-binding flavodoxins, and a detailed kinetic, biophysical, and spectroscopic analysis is presented. The capacity of both flavodoxins to pass electrons to BioI is established, and their relative efficiencies in driving P450 catalysis is compared with that of the host ferredoxin, Fer.

EXPERIMENTAL PROCEDURES

Molecular Biology. Isolation of Chromosomal DNA. Chromosomal DNA from *B. subtilis* 168 was prepared by a cesium chloride centrifugation method. LB medium (2 × 400 mL) was inoculated with an overnight culture (25 mL) of *B. subtilis* and grown to high density (37 °C, 200 rpm, 10 h). Cells were then harvested by centrifugation (9000 rpm,

20 min, 4 °C). The cell pellet was resuspended in 10 mL of sterile GTE buffer (40 mM Tris·HCl, 50 mM glucose, 10 mM EDTA, pH 8.0) and repelleted. After resuspending in 4 mL of GTE, lysozyme (0.5 mL, 5 mg/mL stock) and RNase (0.2 mL, 2 mg/mL stock) were added, and the mixture was incubated (37 °C, 30 min). Triton X-100 (0.7 mL, 8% [v/v] in GTE) and Pronase (0.3 mL, 5 mg/mL stock) were added, and the suspension was incubated (37 °C, 1 h). Cesium chloride (5.92 g, ca. 1% w/v) was added, and the solution was swirled to dissolve it. Ethidium bromide (0.3 mL, 10 mg/mL) was added, and the resulting pink solution was poured into Beckman Optiseal tubes (4.9 mL) and centrifuged (55 000 rpm, 20 °C, 16 h) to resolve the chromosomal DNA.

The banded chromosomal DNA was visualized under UV light and extracted using a sterile syringe. After transfer to a siliconized glass tube, the ethidium bromide was removed by repeated extraction with 1-butanol saturated with sterile TE buffer [10 mM Tris·HCl, 1 mM EDTA, pH 7.5] containing 5 M NaCl. Water (2 volumes) was added to the colorless aqueous layer, followed by 2 volumes of ethanol (95% v/v) prechilled at −20 °C. The precipitated DNA was recovered by centrifugation (15 000 rpm, 15 min, 4 °C), washed with chilled 75% v/v ethanol, and stored at 4 °C for 16 h. The pellet was resuspended (sterile distilled water, 1 mL), and water-saturated phenol (pH 8.0, 1 mL) was added. The aqueous layer was retained and extracted again (water-saturated phenol/chloroform, 1:1 v/v, 1 mL), and the DNA was precipitated again by addition of prechilled ethanol (95% v/v, 2.5 volumes). The DNA was pelletted by centrifugation (4000 rpm, 10 min); the pellet washed (75% v/v ethanol, −20 °C) and dried under vacuum. The dried pellet was resuspended in sterile TE (1 mL) and stored at 4 °C until used. The purity of the chromosomal DNA prepared was analyzed by gel electrophoresis, and its concentration was determined from absorption at 260 nm (*34*).

Amplification and Cloning of the ykuN and ykuP Genes. The *ykuN* and *ykuP* genes were cloned using the polymerase chain reaction (PCR) with *B. subtilis* chromosomal DNA as the template. Oligonucleotide primers for the amplification of the *ykuN* and *ykuP* genes were designed through analysis of the respective gene sequences and the surrounding regions, using the "Subtilist" web server (http://genolist.pasteur.fr/SubtiList/). Oligonucleotides were synthesized at the Protein and Nucleic Acid Chemistry Laboratory (PNACL) at the University of Leicester. For YkuN, the two primers used were as follows: ykuN-N-term, ATA**ACCATGG**CTAAAGCCTTGATTACATATG; ykuN-C-term: CC**GGATCC**TTTATGAAACATGGATTTTTTCC. The nucleotides set in bold indicate engineered restriction sites for the enzymes *Nco*I and *Bam*HI, respectively, at the 5′ ends of the oligonucleotides, introduced to facilitate subsequent cloning into expression vectors. The underlined nucleotides represent deviations from absolute identity with the template DNA. For YkuP, the two primers were ykuP-N-term, GAAT**CCATGG**CGAAGATTTTGCTCGTTTATG, and ykuP-C-term, CC**GGATCC**TGATTTTCTACCTCATTACTGT.

The PCR reactions were carried out using the Roche Expand High Fidelity PCR kit and a Perkin-Elmer PCR cycler. PCR was performed in 0.5 mL Eppendorf tubes using a 100 μL reaction volume. Template DNA (1 μL, 50−100 ng), primers (1 μL, 50 pmol), and the dNTP mix were mixed in one tube (made up to 50 μL with sterile distilled water) and, immediately prior to initiating the PCR, transferred to a second tube that contained the High Fidelity enzyme mix (*Taq* and *Pwo* polymerase, 0.75 μL) and the manufacturer's buffer (10 μL, containing 1.5 mM magnesium chloride) made up to 50 μL with sterile distilled water. PCR reactions were run for 10 cycles of 94 °C, 30 s; 72 °C, 120 s; and 50 °C, 30 s. Thereafter, a further 20 cycles were run with the elongation step extended by 5 s (94 °C, 30 s; 72 °C, 125 s; and 50 °C, 30 s). The PCR products were analyzed by running a sample (2 μL) on an agarose gel (0.8%) and staining with ethidium bromide. The remaining PCR products (98 μL) were purified using a Qiagen MinElute Column purification kit. Recovery of the product eluted from the column (20 μL in 10 mM Tris·HCl, pH 7.5) was verified by agarose gel electrophoresis, as above.

The purified PCR products containing the *ykuN* and *ykuP* genes were digested with *Nco*I and *Bam*HI (NEB) using the buffers supplied by the manufacturer (approximately 4 μg of DNA, 10 units of enzyme, 37 °C, 5 h incubation). The digested DNA samples were resolved by agarose gel electrophoresis (0.8% agarose) and visualized under UV illumination, and the appropriate bands were excised and purified from the agarose using a Qiagen Gel Extraction Kit, as above. The concentration and purity of the recovered digested DNA was checked by agarose gel electrophoresis as detailed above by reference to standards of known concentration. The expression vector pET16b (Novagen) was prepared from a 50 mL LB culture of *E. coli* TG1 transformants using a Qiagen plasmid preparation kit. The vector (20 μL [approximately 4.8 μg] in sterile distilled water) was mixed with restriction enzymes (2 units each of *Nco*I and *Bam*HI) and appropriate buffer, along with shrimp phosphatase (2 μL, 5 units), and the mixtures were diluted with sterile distilled water (100 μL total volume in both cases). Digestions were performed at 37 °C for 5 h. The digested plasmids were resolved by agarose gel electrophoresis and purified as above.

Digested pET16b vector DNA (50−100 ng, 2 μL), ligation buffer (10 mM Tris·HCl, pH 7.2, 1 mM EDTA, 10 mM $MgCl_2$, 10 mM DTT, and 1 mM ATP, 2 μL) and T4 DNA ligase (2 μL, 800 units) were mixed with varying amounts of the *ykuN* and *ykuP* PCR products (1, 2, and 4 μL [50, 100, and 200 μg]). Sterile distilled water was added to a final volume of 10 μL, and the reaction mixtures were incubated at 16 °C for 16 h. *E. coli* XL1-Blue competent cells (50 μL) were transformed with the ligation mixtures (2 μL) by electroporation (200 Ω, 1.8 V). SOC medium (2 mL) was added to the transformed cells, which were then incubated with agitation (37 °C, 45 min) before being spread onto agar plates (LB containing 50 μg ml^{-1} ampicillin) and left to grow overnight at 37 °C. Colonies from the transformation plates were cultured, and plasmids were prepared as described above. Clones of *ykuN* (pETYkuN) and *ykuP* (pETYkuP) were verified by digestion of the DNA with *Nco*I and *Bam*HI, and the sequences of clones selected for further use were verified by Sanger dideoxy sequencing (*35*).

Expression and Purification of the YkuN and YkuP Proteins. Transformant *E. coli* cells (HMS174 (DE3) pLysS, Novagen) carrying the pETYkuN and pETYkuP expression plasmids were grown on large scale (6 L, 12 × 0.5 L in 2 L flasks) in LB media containing ampicillin (100 μg/mL) at

37 °C for 24 h with vigorous shaking (250 rpm). Isopropyl-β-D-thiogalactopyranoside (IPTG) (0.5 mM) was added in late logarithmic phase of growth (OD_{600} = 1.0) to induce flavodoxin expression. The cells were harvested by centrifugation (5000 rpm, 20 min), and the blue-colored cell pellets were frozen (−20 °C, overnight). Thawed cells were resuspended in a minimal volume of buffer A (50 mM Tris·HCl, pH 7.2) containing 1 mM EDTA and sonicated on ice using a Bandelin Plus sonicator (10 × 20 s bursts on 50% power, interspaced by 2 min). Pale blue cell suspensions were centrifuged at high speed (15 000*g*, 40 min, 4 °C) to pellet insoluble cellular debris, leaving blue supernatants containing the required flavodoxin (predominantly in its semiquinone form).

Ammonium sulfate was added slowly with stirring to the soluble cell extracts (ca. 100 mL, chilled on ice) to give a final concentration of 1.5 M (YkuN) or 2.0 M (YkuP). The flavodoxins remained in solution during this treatment. Precipitated proteins were removed by centrifugation (15 000 rpm, 40 min, 4 °C), and the supernatant containing the flavodoxins was loaded directly onto a phenyl Sepharose column (5 cm × 30 cm) pre-equilibrated with an ammonium sulfate solution of the same molarity in 50 mM Tris·HCl, pH 7.0 (buffer B). The phenyl Sepharose column was washed with three column volumes of buffer B plus the relevant ammonium sulfate concentration (0.5 mL/min), prior to eluting the flavodoxin with a linear gradient (1.5 or 2.0 M ammonium sulfate to 0.5 M in buffer B, 2 column volumes). Fractions were analyzed by UV/visible spectroscopy, and those containing flavodoxin with an A_{280}/A_{461} ratio of 10:1 or lower were retained. The fractions were pooled and concentrated to ca. 50 mL by ultrafiltration (Centriprep concentrators, 10 kDa cutoff, Millipore). The concentrated solutions were dialyzed twice against buffer A (2 L, 4 °C, 6 h) prior to loading onto a DEAE Sephacel column (approximately 5 cm × 30 cm) pre-equilibrated with the same buffer. After extensive washing of the column with buffer A (4 column volumes, 0.2 mL/min), the protein was eluted with a linear salt gradient (50 mM to 1 M KCl in buffer A, 2 column volumes). YkuN eluted at ca. 400 mM KCl and YkuP at ca. 450 mM KCl. The spectra of the most intensely colored fractions were analyzed, and those containing the highest flavin/protein ratio (A_{280}/A_{461} < 8) were retained and concentrated by ultrafiltration (as previously). The resulting concentrated protein fractions were dialyzed twice against buffer A (2 L, 4 °C, 6 h) prior to loading onto a Q-Sepharose column (approximately 5 cm × 30 cm) pre-equilibrated in buffer A. After the column was washed with buffer A (4 column volumes, 0.15 mL/min), the proteins were eluted with a linear salt gradient (50−500 mM KCl in buffer A, 2 column volumes). YkuN was observed to elute at ca. 250 mM KCl and YkuP at ca. 300 mM KCl. As previously, the most intensely yellow colored fractions were retained and concentrated by ultrafiltration (Centricon and Amicon concentrators, 10 kDa cutoff) to approximately 20 mg/mL. At this stage, both flavodoxins were substantially >90% pure. To produce electrophoretically homogeneous YkuN and YkuP proteins, a final gel filtration step using Sephadex S-200 resin (column dimensions ~4 cm × 1 m) was used. Small aliquots of the concentrated flavodoxin preparations (ca. 1 mL) were run through the column in buffer A (0.10 mL/min). Fractions were collected, pooled, and analyzed spectrophotometrically as before. YkuN with an A_{280}/A_{461} nm ratio of ~6:1 were regarded as pure (as confirmed by SDS−PAGE), and similarly pure YkuP had an A_{280}/A_{461} nm ratio of ~3.5:1. The final protein solutions were concentrated as previously described to ~1 mM and dialyzed against buffer A containing 50% v/v glycerol at 4 °C. Pure flavodoxins were stored in small aliquots (~ 50−100 μL) at −80 °C. All purification steps were done in a cold room (at 4 °C), and all solutions contained phenylmethylsulfonyl fluoride (1 mM) and benzamidine hydrochloride (1 mM) to minimize proteolysis.

Expression and Purification of E. coli Flavodoxin NADP$^+$ Oxidoreductase (FLDR). E. coli FLDR was purified to provide a NADPH-dependent reductase system for mediation of electron transfer to YkuN and YkuP for transient kinetic and steady-state studies. FLDR was expressed and purified largely as described previously (*32*). Induction with IPTG was found to be unnecessary for high levels of production of FLDR. Following purification by ion exchange chromatography on DEAE Sepharose and Q-Sepharose resins, a final affinity purification step on a 2′,5′-ADP Sepharose column was used to prepare homogeneous FLDR. Fractions from the affinity purification process with A_{280}/A_{456} ratios of <6:1 were concentrated by ultrafiltration to ~0.5 mM final concentration, dialyzed extensively against buffer A with 50% (v/v) glycerol, and stored at −80 °C. All purification steps were done in a cold room (at 4 °C), and all solutions contained phenylmethylsulfonyl fluoride (1 mM) and benzamidine hydrochloride (1 mM) to minimize proteolysis.

Transient Kinetic Studies: Electron Transfer from YkuN and YkuP to P450 BioI. The rate of the single electron transfer from the *B. subtilis* flavodoxins to P450 BioI was measured by stopped-flow absorption using an Applied Photophysics SX18MV UV−visible stopped-flow instrument coupled to a photodiode array UV/visible detector. Experiments were carried out under anaerobic conditions (<5 ppm O_2) in a glovebox (Belle Technology). P450 BioI was purified as described in the accompanying manuscript (*36*). BioI, YkuN, and YkuP proteins were prepared separately in 50 mM potassium phosphate (pH 7.0) that had been degassed (argon sparged) and saturated with carbon monoxide to give solutions of the flavodoxins YkuN or YkuP (80 μM) and BioI (4.0 μM). To different samples of BioI, palmitoleic acid (final concentration 20 μM) or testosterone (final concentration 60 μM) was added to convert the P450 to an extensively high-spin or low-spin form, respectively (*36*). Prior to performing the stopped-flow experiment, flavodoxins were reduced by titration with sodium dithionite using the minimal amount of reductant required to produce full reduction of the flavoproteins (by comparison with spectral data from redox titrations, see below). Excess dithionite was removed by gel filtration (BioRad 10DG column) in the anaerobic glovebox prior to stopped-flow mixing of reduced YkuN or YkuP (4−50 μM) with BioI (1.8 μM) in its fatty acid (palmitoleate)-bound or testosterone-bound forms at 30 °C. Entire spectra were recorded (250−750 nm) using the photodiode array facility. To rule out any significant spectral changes to BioI resulting from photobleaching, an identical sample of the P450 was also mixed with a buffer blank and the spectrum was recorded over 8 min. These data were subtracted from those collected in the presence of the flavodoxins to produce corrected rates that are specific for flavodoxin-dependent electron transfer. The rate of electron

transfer from YkuN or YkuP to P450 BioI was followed using the accumulation of absorption at 448 nm (A_{448}) corresponding to formation of the ferrous/CO complex of the P450. Rates were determined by analyzing spectra with global analysis software (Applied Photophysics ProKin software). Observed rates were plotted against the relevant flavodoxin concentration, and data were fitted (using Microcal Origin) to eq 1 to obtain the apparent P450/flavodoxin binding constants (K_d values) and the apparent limiting rates for electron transfer (k_{red}) from YkuN or YkuP to P450 BioI in its different states.

$$k_{obs} = (k_{red}/2E_t)(S + E_t + K_d) - (((S + E_t + K_d)^2 - 4SE_t)^{0.5}) \quad (1)$$

In eq 1, k_{obs} is the observed rate of electron transfer at flavodoxin concentration S, E_t is the total P450 BioI concentration, and K_d is the apparent dissociation constant for the productive flavodoxin/P450 complex.

Transient Kinetic Studies: Electron Transfer between FLDR and the B. subtilis Flavodoxins. The rate of electron transfer from the *E. coli* FLDR to the *B. subtilis* YkuN and YkuP flavodoxins was measured anaerobically by stopped-flow mixing, as described above. Proteins (YkuN or YkuP, 30 μM, and FLDR, 225 μM) were prepared in 50 mM potassium phosphate (pH 7.0) and degassed (argon sparged). FLDR was reduced by the addition of the minimal amount of NADPH (~4 mM) to generate the hydroquinone form immediately prior to the experiment. The reduced FLDR and oxidized YkuN or YkuP were mixed in the stopped-flow instrument at 30 °C, and the spectra were recorded (250−750 nm). Photobleaching effects were accounted for by mixing identical samples of flavodoxin against buffer blanks and recording spectra over 8 min. A degree of bleaching of the FMN signal was observed over this time scale, and (as described above) the data were subtracted from those accumulated in experiments involving flavodoxin/FLDR mixing. FLDR (225−7.5 μM) was mixed with YkuN or YkuP (30 μM), and the interprotein FAD-to-FMN rate was determined by analysis of the accumulation of absorption increase at 591 nm, specific for the neutral (blue) semiquinone form of the FMN of the flavodoxins. Rate data at 591 nm were fitted accurately to a single-exponential process (using Spectrakinetics software). Global analysis of entire spectra accumulated was also performed (using Applied Photophysics ProKin software). Observed rates were plotted versus FLDR concentration and fitted to eq 1 in Origin (as described above) to define apparent K_d values for FLDR/flavodoxin interactions and for the limiting rates of interflavin electron transfer (k_{red}) between FLDR and YkuN or YkuP.

Verification of Flavodoxin-Supported Fatty Acid Hydroxylation by P450 BioI. To determine whether electron transfer to BioI from the *E. coli* NADPH−flavodoxin reductase via *E. coli* flavodoxin or the YkuN and YkuP flavodoxins from *B. subtilis* was coupled to oxidative catalysis of BioI, assay systems were set up containing the relevant enzyme partners. The turnover of lauric acid, myristic acid, 13-methyl myristic acid, palmitic acid, and palmitoleic acid was investigated. Conditions used in all cases were those optimized for turnover of myristic acid. The catalytic hydroxylation of myristic acid by BioI was carried out in 25 mL sterilin reaction vials (12 mL total reaction volume) in 20 mM MOPS buffer (pH 7.0) containing 100 mM KCl at room temperature (approximately 23 °C) with continuous stirring. Myristic acid (4.0 μmol) was suspended in the buffer, and the following proteins were added: BioI (80 nmol), YkuN or YkuP (20 nmol), and *E. coli* flavodoxin reductase (20 nmol). The resulting orange-colored mixtures were stirred (5 min, 23 °C) prior to the addition of NADPH (12.0 μmol). The reaction was allowed to proceed for 16 h before being terminated by acidification (1 M HCl, pH 2.0, few drops). The fatty acids were extracted into chloroform (2 × 3.0 mL); the organic layers were combined, back-extracted with brine (1 × 3.0 mL), dried (using magnesium sulfate) and evaporated to dryness. The off-white residue was resuspended in methanol and analyzed by electrospray mass spectrometry. Mass spectra were obtained in EI mode (70 eV ionization) using a Micromass Quattro triple quadrupole mass spectrometer.

Steady-State Kinetic Analysis of YkuN or YkuP Interactions with P450 BioI. To further assess the ability of the two *B. subtilis* flavodoxins to act as catalytically functional electron donors to BioI, steady-state kinetic studies were performed. A solution was prepared containing BioI (2.3 nmol) and *E. coli* flavodoxin reductase (30 nmol) in aerobic 50 mM potassium phosphate (pH 7.0, total volume of 1.0 mL), and mixed with varying amounts of the YkuN or YkuP flavodoxins (0−30 μM). Fatty acid substrate (palmitoleic acid, lauric acid, myristic acid, or palmitic acid) or the steroid testosterone (50 μM) was added, and the solution was allowed to equilibrate for 2 min at 30 °C. NADPH (200 μM) was injected, and the solution was mixed prior to recording the oxidation of NADPH at 340 nm ($\epsilon_{340\ nm}$ = 6210 M^{-1} cm^{-1}) over periods of up to 3 min in a Cary UV-50 Bio scanning spectrophotometer. Initial reaction rates were determined in duplicate at each concentration of flavodoxin. NADPH oxidation rates (expressed as moles of NADPH oxidized per minute per mole of P450) were plotted versus the relevant concentration of flavodoxin. Data were fitted to rectangular hyperbolae using Origin (Microcal) to derive the apparent k_{cat} value for the systems and to determine apparent binding constants (K_M values) for the interactions between the flavodoxins and P450 BioI in steady-state turnover.

Determination of Uncoupling in the P450 BioI Reactions with YkuN or YkuP. To determine the degree of uncoupling that occurs during the steady-state turnover of myristic acid by BioI, a colorimetric assay was used (*37*). Following steady-state analysis (see above), complete consumption of NADPH was ensured (reaction was run until no further change in A_{340} occurred). A solution of *o*-dianisidine (8 mM, 20% v/v in Triton X-100) was prepared and added (50 μL) to the reaction mixture. Horseradish peroxidase (50 mg/mL, 13.5 units/μL) was added (2 μL), and the solution was mixed by inversion and incubated for 2 min at 30 °C. The increase in absorption at 440 nm was recorded, and the quantity of peroxide present was determined using the extinction coefficient ϵ_{440} = 11 600 M^{-1} cm^{-1} (*37*).

Spectroscopic Studies: Electron Paramagnetic Resonance. EPR spectra were recorded on an X-band ER-200D spectrometer (Bruker Spectrospin) fitted with a liquid helium flow cryostat (ESR-9, Oxford Instruments). The samples were prepared in 50 mM Tris·HCl (pH 7.0). The protein concentrations were 1.0 mM for both YkuN and YkuP. Spectra were

recorded at 10 K with microwave power = 2.01 mW and modulation amplitude = 10.0 G

Spectroscopic Studies: Circular Dichroism. Far UV circular dichroism (CD) spectra (190−260 nm) were recorded for YkuN and YkuP at 20 °C on a JASCO J-750 spectropolarimeter purged with nitrogen. All samples were in 50 mM Tris·HCl, pH 7.2. The concentration of the YkuN and YkuP flavodoxins used was 0.1 mg/mL.

Structural Stability and Flavin Binding in YkuN and YkuP: Stability of Structure and Flavin Binding to the Chaotrope Guanidinium Chloride. The effects of guanidinium chloride (GdmCl) on secondary and tertiary structure of YkuN and YkuP and on the binding of their FMN cofactor were investigated. YkuN or YkuP were made up in potassium phosphate (50 mM, pH 7.0, varying volumes and flavodoxin concentrations), and the appropriate volume of GdmCl (8 M in the same buffer) was added to give the required concentration of the chaotrope (0−7 M). After addition of GdmCl, solutions were incubated at room temperature (ca. 23 °C, 15 min) and then analyzed by spectrophotometry (spectra recorded between 300 and 750 nm, 1 cm path length quartz cell, Cary UV-50 Bio spectrophotometer, total sample volume = 1.0 mL, approximately 12 nmol protein), tryptophan fluorescence (excitation at 290 nm, emission collected between 300 and 400 nm, 1 cm path length polished quartz cell, excitation and emission slit widths set at 10 nm on a Cary Eclipse fluorimeter [Varian], total sample volume = 3.0 mL, approximately 3.0 nmol protein), FMN fluorescence (excitation at 450 nm, emission collected between 500 and 600 nm, excitation and emission slit widths set at 5 nm on a Cary Eclipse fluorimeter, total sample volume = 3.0 mL, approximately 3.0 nmol protein), and far UV CD (spectra collected between 190 and 260 nm in a quartz cell of 0.1 cm path length on a JASCO J-750 spectropolarimeter, total sample volume = 0.4 mL, approximately 570 nmol protein). Plots of absorption, fluorescence, or CD change versus GdmCl concentration described sigmoids and were fitted to the Hill function (see accompanying paper, ref *36*) to define the midpoint concentration of GdmCl (K^U) required to induce 50% of the maximal change, reflecting unfolding of secondary or tertiary structure or displacement of flavin from its native binding site.

Structural Stability and Flavin Binding in YkuN and YkuP: Generation of the Apoprotein Forms of the Two B. subtilis Flavodoxins. Samples of YkuN and YkuP flavodoxins (2.0 μmol) were dialyzed into 50 mM potassium phosphate (pH 7.0) for 4 h at 4 °C. Trichloroacetic acid (TCA, 5% w/v) was added to the protein solutions, and the resulting yellow suspensions were incubated on ice (30 min). The protein was recovered by centrifugation (15 000*g*, 20 min, 4 °C) to yield a small off-white pellet. The apoprotein pellet was resuspended into 50 mM potassium phosphate (pH 7.0) and dialyzed against the same buffer (2 L, 16 h, 4 °C) to yield a clear solution. The apoprotein solution was then dialyzed against the same buffer containing 50% v/v glycerol (1 L, 6 h, 4 °C), divided into small aliquots (200 μL), and frozen at −20 °C. Absence of flavin was demonstrated by lack of absorption in the near-UV−visible range (300−700 nm). Samples were used experimentally within 1 week of preparation (*38*, *39*).

Structural Stability and Flavin Binding in YkuN and YkuP: Differential Scanning Calorimetry Studies. Differential scanning calorimetry (DSC) experiments were performed to characterize the heat-induced conformational transition of the *B. subtilis* flavodoxins YkuN and YkuP. DSC allows the unfolding transition midpoint temperature (T_m) to be determined. Hence useful information on the thermal stability of the protein can be obtained. All DSC scans were performed using a MicroCal VP-DSC (MicroCal) at a heating scan rate of 1 °C/min (unless otherwise stated). The DSC was interfaced to a Gateway PIII computer, and data acquisition was achieved using Origin 5.0 (MicroCal LLC, Northampton MA). The reference cell was always filled with a buffer solution, and instrumental baselines were measured by placing buffer in both cells and scanning up in temperature. Buffer baselines were subtracted from scans of the protein prior to data analysis using Origin 5.0. Stock solutions of YkuN and YkuP were dialyzed against 2 L of 50 mM potassium phosphate (pH 7.5) for 24 h. The dialysis buffer was stored for use in reference experiments. Stock solutions of both proteins at a concentration of 0.36 mM were aliquoted for DSC experiments. In all cases, initial DSC scans were manually stopped just after T_m. The samples were then cooled back to room temperature, and the scans were repeated (a standard procedure for checking the reversibility of protein unfolding).

Data analysis was carried out as follows: Raw DSC data for the protein scan and for a buffer versus buffer baseline were opened in Origin 5.0, and the buffer baseline was subtracted from the protein scan. The software was then used to fit a spline baseline to the data using pre- and posttransition baselines to subsequently integrate the endotherms and hence evaluate the calorimetric enthalpy (ΔH_{cal}). This baseline-corrected scan was then normalized for scan rate and molar concentration of protein. Values for T_m and ΔH_{cal} were obtained directly from the scan by simple integration. Analysis of the scan line shape using a non-two-state model incorporated in Origin was used to determine the van't Hoff enthalpy (ΔH_{vH}).

Structural Stability and Flavin Binding in YkuN and YkuP: Determination of Affinity of FMN for the YkuN and YkuP Apoproteins. A solution of FMN (0.1 μM, high-purity HPLC-purified cofactor) was prepared in potassium phosphate (50 mM, pH 7.0, 3 mL total volume). Successive aliquots of YkuN or YkuP apoprotein solutions (120−240 μM, generated as described above, 1 μL per addition) were added to the FMN solution. The fluorescence emission of the FMN cofactor was measured using a Cary Eclipse instrument. Excitation was at 450 nm, emission was recorded from 500 to 600 nm, and excitation and emission slit widths were both set at 5 nm. The quenching of the flavin fluorescence observed on YkuN or YkuP binding was corrected for dilution and for the effects of addition of apoprotein in the absence of FMN. Riboflavin binding was also assessed using the same procedure, as described previously (*38*, *40*). Data were fitted to eq 2 (a modified version of eq 1) to define the apparent K_d values for FMN binding to YkuN and YkuP.

$$F_{obs} = (F_{max}/(2C_t))([Apo] + C_t + K_d) - ((([Apo] + C_t + K_d)^2 - 4[Apo]C_t)^{0.5}) \quad (2)$$

In eq 2, F_{obs} is the fluorescence change observed at the relevant concentration of apoflavodoxin ([Apo]) added. C_t is the total amount of FMN cofactor in the assay. F_{max} is the

maximal change in fluorescence observed at saturation, and K_d is the dissocation constant for the binding of FMN to the apoflavodoxin.

Analysis of P450 BioI/Flavodoxin Interactions by Spectrophotometric and Fluorescence Titrations. Binding of the YkuN and YkuP flavodoxins induced a small shift in the Soret band of P450 BioI toward the high-spin form (i.e., to shorter wavelength). To a solution of BioI (1.6 nmol) in buffer A (0.78 mL) aliquots of the flavodoxins (1.0 μL, 40 μM) were added, and the resulting UV/visible spectra recorded (between 250 and 750 nm) at 25 °C on a Cary UV-50 Bio spectrophotometer. The extent of absorption shift in the Soret band was plotted against the concentration of flavodoxin, and the data were fitted to eq 2 using Origin software (Microcal).

Interaction of the flavodoxins with P450 BioI was also analyzed by the quenching of flavin fluorescence, taking advantage of the solvent-exposed nature of their FMN cofactor. BioI (2.1 nmol) was added to potassium phosphate (50 mM, pH 7.0, total volume 3.0 mL), aliquots of flavodoxin were added (0.5 μL, 0.15 mM stock solution in same buffer), and the flavin emission spectra were measured (excitation at 450 nm, emission collected between 500 and 600 nm, excitation and emission slit widths both set at 5 nm on the Cary Eclipse instrument) at 25 °C. The assay was repeated in the absence of BioI, and the relevant spectra were subtracted from those with BioI present to compensate for nonspecific changes in flavin emission. The quenching of flavin emission (at 528 nm) was plotted against the concentration of flavodoxin added, and the data were analyzed using Origin software.

Potentiometric Titrations of YkuN and YkuP. All redox titrations were carried out in an anaerobic glovebox (Belle technology, Portesham, England) under a nitrogen atmosphere with oxygen levels maintained at <5 ppm. Redox titrations were carried out for both YkuN and YkuP (typically in the range 10−40 μM protein) at 25 ± 2 °C using the method of Dutton and essentially as described previously (*8*, *41*, *42*). Redox titration buffer (100 mM potassium phosphate, pH 7.0) was deoxygenated by bubbling extensively with O_2-free argon and degassed prior to transfer to the glovebox. Oxygen was removed from flavodoxin samples by passing concentrated stock solutions through a Bio-Rad Econo-pac 10DG gel filtration column in the glovebox, which had been preequilibrated with redox titration buffer containing 5% (v/v) glycerol. Titrations were performed in both reductive and oxidative directions to ensure lack of hysteresis. Absorption changes during the titrations were monitored via a fiber optic absorption probe (Varian) immersed in the flavodoxin solution in the anaerobic environment and connected to a Cary UV-50 Bio UV−visible spectrophotometer (Varian) outside the glovebox. Mediators were added to facilitate electrical communication between enzyme and electrode prior to titration. Typically, 2 μM phenazine methosulfate, 5 μM 2-hydroxy-1,4-naphthoquinone, 0.5 μM methyl viologen, and 1 μM benzyl viologen were included to mediate in the range between +100 and −480 mV, as described previously (*8*, *41*).

Data were analyzed by plotting the absorbance at an appropriate wavelength, corresponding to the maximal absorbance change between oxidized, semiquinone, and reduced forms, against the potential. A two-electron Nernst function (eq 3) was then fitted to the data to describe the transitions between quinone, semiquinone, and hydroquinone forms of the FMN, and the midpoint potentials were calculated from these data fits. Equation 3 represents a two-electron redox process derived by extension to the Nernst equation and the Beer−Lambert Law, as described previously (*8*, *41*).

$$A = \frac{a10^{(E-E_1')/59} + b + c10^{(E_2'-E)/59}}{1 + 10^{(E-E_1')/59} + 10^{(E_2'-E)/59}} \quad (3)$$

In eq 3, A is the total absorbance; a, b, and c are component absorbance values contributed by the FMN in the oxidized, semiquinone, and reduced states; E is the observed potential; E_1' and E_2' are the midpoint potentials for oxidized/semiquinone and semiquinone/reduced couples of the flavin, respectively.

The midpoint reduction potentials for the flavin couples of YkuN or YkuP and for P450 BioI were also determined by potentiometric analysis of stoichiometric flavodoxin/P450 complexes (12 μM each of either YkuN/BioI or YkuP/BioI). P450 BioI was saturated with the tight-binding fatty acid myristic acid (200 μM) (*16*). Redox titrations were performed as detailed above. The oxidized/semiquinone and semiquinone/hydroquinone potentials for the FMN cofactors in YkuN and YkuP were determined from the change in absorption at 596 nm (YkuN) and 590 nm (YkuP). At these wavelengths, there are minimal contributions from the α/β bands of the P450 heme during reduction of the flavins. Data were fitted to eq 3, as detailed above. The reduction potential for the ferric/ferrous couple of the heme iron was determined from absorption change between the wavelengths of 409 and 392 nm. In this regime, there is minimal contribution from the YkuN or YkuP FMN as it undergoes its semiquinone-to-hydroquinone reduction across a similar potential range as the heme reduction. Data for the heme reduction were fitted to eq 4, describing a single-electron process, as described previously (*41*).

$$A = \frac{a + b10^{(E_1'-E)/59}}{1 + 10^{(E_1'-E)/59}} \quad (4)$$

In eq 4, A is the total absorption change, a and b are component absorbance values contributed by the P450 heme in the oxidized and reduced states; E is the observed potential, and E_1' is the midpoint potential for the ferric/ferrous couple of the heme iron.

RESULTS

Cloning and Sequencing of YkuN and YkuP. The genes encoding the two *B. subtilis* flavodoxins were amplified by PCR from chromosomal DNA, as described in the Experimental Procedures section. Agarose gel electrophoresis revealed product bands of the correct size (~0.59 kbp for *ykuN*, ~0.63 kbp for *ykuP*). Purified PCR fragments were digested with the restriction enzymes *Nco*I and *Bam*HI (exploiting sites engineered into the PCR primers) and cloned into the expression vector pET16b (Novagen). Successful clones were verified by restriction enzyme digestion, and large-scale plasmid preparations were undertaken for DNA sequencing. The sequence of *ykuN* was found to be identical

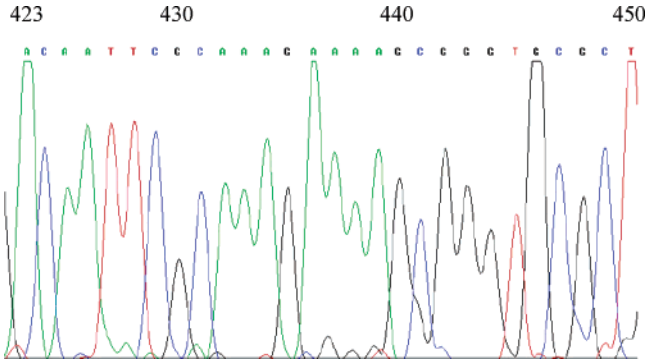

FIGURE 2: DNA sequence of *B. subtilis ykuP*. A section of the DNA sequencing data from a typical *ykuP* clone is shown. The region between nucleotides 423 and 450 (corrected sequence numbers) is indicated. In the original genomic sequence of *B. subtilis* (http://genolist.pasteur.fr/SubtiList/), a string of five "A" nucleotides are present in positions 436−440. Our data show that this is in fact a string of four "A" nucleotides in positions 436−439. The induced frame shift results in a stop codon being introduced at positions 454−456.

to that reported on the SubtiList database (http://genolist-.pasteur.fr/SubtiList/) and to encode a putative protein of 158 amino acids (including initiator methionine) and of molecular mass 17 793 Da. However, the sequence of *ykuP* differed from that previously reported, and the difference was consistent among several clones originating from different PCR reactions. According to the genome sequence data, *ykuP* encodes a putative protein of 178 amino acids (including the initiator methionine) and of molecular mass 20 253 Da. Our sequencing data indicates that there is an "A" nucleotide absent in the sequence at nucleotide position 436 (resulting in a string of four, rather than five, consecutive "A" nucleotides). This results in a change in reading frame from position 436 (amino acid 146) onward and in the predicted translated sequence terminating earlier with a TGA stop codon introduced at positions 454−456 in the sequence (Figure 2). Thus, the corrected *ykuP* gene encodes a putative protein of 151 amino acids with a predicted molecular mass of 16 868 Da. *E. coli* is also known to contain two flavodoxin proteins (FldA and FldB), but these are of rather larger size than those in *B. subtilis*. *E. coli* FldA is a 175 amino acid protein of predicted mass 19 606 Da; FldB is a 173 amino acid protein of predicted mass 19 700 Da.

Despite great similarities in overall tertiary structure, two broad and distinct classes of flavodoxins are recognized. In the "long-chain" flavodoxins, the last of the five β strands of the protein is broken into two segments by an intervening section of approximately 20 amino acid residues (*43*). This segment is absent from the "short-chain" flavodoxins. Thus, the apparent discrepancy between our sequencing data and those from the genomic sequence are not simply resolved on the basis of size comparisons of the "long" and "short" forms of YkuP with other flavodoxins. The "long" form of YkuP is of approximately the correct size to be a member of the "long-chain" family and vice versa for the "short" form. Amino acid alignments (using ClustalW at the EBI web site, http://www.ebi.ac.uk/clustalw/) between the "short" and "long" forms of YkuP and other bacterial flavodoxins (including YkuN) are strongly supportive of YkuP being a short-chain flavodoxin (Figure 3). The alignment shows that the insert present in each of the well-defined long-chain flavodoxins is absent from the *Desulfovibrio vulgaris* and *Clostridium beijerinckii* short-chain flavodoxins and also from YkuN. Moreover, the insert region is not recognized in either the "short" or "long" forms of YkuP. In the "long" form, the additional C-terminal residues appear at the end of the alignment and do not correlate well with residues in any of the other long-chain or short-chain flavodoxins. Alignment data are thus consistent with our sequencing data and with YkuP being a typical short-chain flavodoxin.

Expression and Purification of YkuN and YkuP. Expression of *ykuN* and *ykuP* genes (cloned in the T7 RNA polymerase promoter plasmid pET16b) was investigated in a series of *E. coli* strains with expression induced by addition of IPTG (1 mM) in the logarithmic phase of growth. Efficient expression was achieved in both BL21 (DE3) and HMS174 (DE3) pLysS strains. The latter strain was chosen for preparation of both YkuN and YkuP proteins, since this strain consistently gave slightly higher production levels of the YkuN flavodoxin. SDS−PAGE gel studies showed that levels of flavodoxin expression were maximal by 6−18 h after induction. Thus, HMS174 (DE3)/pETYkuN and HMS174 (DE3)/pETYkuP cultures were typically induced in late afternoon or evening, and cells were harvested the following morning. The cultures yielded blue cell pellets, indicative of the predominance of the neutral blue semiquinone form of the FMN cofactor in the overexpressed flavodoxins.

On breakage of the expression cells, the intensity of the blue color of the YkuP lysate deteriorated, and there was complete conversion to a yellow color typical of oxidized FMN on dialysis of the lysate. A similar phenomenon was observed for the *E. coli* flavodoxin (FldA), which was also purified for comparisons with YkuN or YkuP. By contrast, YkuN remained in its blue semiquinone state well beyond these stages of processing, only converting to the yellow oxidized (quinone) form fully following immobilization on Q-Sepharose resin and extensive washing with aerated buffer as a prelude to application of a salt gradient. It is thus likely that the YkuN blue semiquinone shows lower reactivity with oxygen than does the YkuP species. Potentiometric studies (see below) indicate that any differences in semiquinone reactivity with oxygen must have their origin in kinetics of reactivity, rather than in altered thermodynamics of the flavin system. It should be noted that we cannot rule out that the difference in oxygen reactivity between YkuN and YkuP may result from differences in disproportionation rates between the semiquinone species, forming hydroquinone species that reoxidize very rapidly. However, the potentiometric analyses below indicate that there is a large thermodynamic barrier to hydroquinone formation in both flavodoxins.

Both YkuN and YkuP were purified to homogeneity by successive hydrophobic affinity, ion exchange, and gel filtration steps. The N-terminal amino acid sequences of YkuN (AKALITY) and YkuP (AKILLV) were determined. These data are consistent with the predicted sequences and indicate that the initiator methionine residue is removed from both *B. subtilis* flavodoxins on expression in *E. coli*. Figure 4 shows an SDS−PAGE gel of purified YkuN and YkuP proteins. The gel confirms that both proteins are purified as unique species with no significant proteolysis evident in either case. However, the electrophoretic mobilities of YkuN and YkuP are rather different. Based on gel migration, the mass of YkuN is estimated at ~17 kDa, consistent with the predicted molecular mass of 17.7 kDa (with methionine

```
YkuP long          MAKILLVYATMSGNTEAMADLIEKGLQEALAEVDRFEAMDIDDAQLFTDYDHVIMGTYTW 60
YkuP short         MAKILLVYATMSGNTEAMADLIEKGLQEALAEVDRFEAMDIDDAQLFTDYDHVIMGTYTW 60
YkuN               MAKALITYASMSGNTEDIAFIIKDTLQEYELDIDCVEINDMD-ASCLTSYDYVLIGTYTW 59
A. variabilis      SKKIGLFYGTQTGKTESVAEIIRDEFG---NDVVTLHDVSQAEVTDLNDYQYLIIGCPTW 57
Synechococcus      -SKIGLFFGTQTGNTEELAQAIQAAFGG--SDIVELFDVAEVDIEALRDFDQLIIGCPTW 57
E. coli FldB       -MNMGLFYGSSTCYTEMAAEKIRDIIG---PELVTLHNLKDDSPKLMEQYDVLILGIPTW 56
E. coli FldA       -AITGIFFGSDTGNTENIAKMIQKQLG---KDVADVHDIAKSSKEDLEAYDILLLGIPTW 56
C. crispus         --KIGIFFSTSTGNTTEVADFIGKTLGA--KADAPIDVDDVTDPQALKDYDLLFLGAPTW 56
D. vulgaris        MPKALIVYGSTTGNTEYTAETIARELADAGYEVDSRDAASVEAGGLFEGFDLVLLGCSTW 60
C. beijerinckii    ---MKIVYWSGTGNTEKMAELIAKGIIESGKDVNTINVSDVNIDELLN-EDILILGCSAM 56
                        : : : :  *   *  *   :                    :   : ::*  :

YkuP long          GDG----DLPDEFLD-LVEDMEEIDFSGKTCAVFGSGDTA--YEFFCGAVDTLEAKIKER 113
YkuP short         GDG----DLPDEFLD-LVEDMEEIDFSGKTCAVFGSGDTA--YEFFCGAVDTLEAKIKER 113
YkuN               GDG----DLPYEAED-FFEEVKQIQLNGLKTACFGSGDYS--YPKFCEAVNLFNVMLQEA 112
A. variabilis      NIG----ELQSDWEG-LYSELDDVDFNGKLVAYFGTGDQIGYADNFQDAIGILEEKISQR 112
Synechococcus      NVG----ELQSDWEA-LYDDLDDVDFSGKTIAYFGAGDQVGYADNFQDAMGVLEEKITSL 112
E. coli FldB       DFG----EIQEDWEA-VWDQLDDLNLEGKIVALYGLGDQLGYGEWFLDALGMLHDKLSTK 111
E. coli FldA       YYG----EAQCDWDD-FFPTLEEIDFNGKLVALFGCGDQEDYAEYFCDALGTIRDIIEPR 111
C. crispus         NTGADTERSGTSWDEFLYDKLPEVDMKDLPVAIFGLGDAEGYPDNFCDAIEEIHDCFAKQ 116
D. vulgaris        GDD--SIELQDDFIP-LFDSLEETGAQGRKVACFGCGDSS--YEYFCGAVDAIEEKLKNL 115
C. beijerinckii    GDEV---LEESEFEP--FIEEISTKISGKKVALFGSYGWGD-----GKWMRDFEERMNGY 106
                              .          .   ..   * :*  .           :  :.  :

YkuP long          GGDIVLP----------------------SVKIENNPEGEEEEE-LINFGRQFAKKKRVR 150
YkuP short         GGDIVLP----------------------SVKIENNPEGEEEEE-LINFGRQFAKKS--G 148
YkuN               GAAVYQE----------------------TLKIELAPETDEDVESCRAFARGFLAWADYM 150
A. variabilis      GGKTVGYWSTDGYDFNDSK-ALRNGK-FVGLALDEDNQSDLTDDRIKSWVAQLKSEFGL- 169
Synechococcus      GGKTVGQWPTAGYDHSESK-AERDGK-FVGLAIDEDNQPELTAERIQAWVAQLKPAFGL- 169
E. coli FldB       GVKFVGYWPTEGYEFTSPKPVIADGQLFVGLALDETNQYDLSDERIQSWCEQILNEMAEH 171
E. coli FldA       GATIVGHWPTAGYHFEASK-GLADDDHFVGLAIDEDRQPELTAERVEKWVKQISEELHLD 170
C. crispus         GAKPVGFSNPDDYDYEESK-SVRDGK-FLGLPLDMVNDQIPMEKRVAGWVEAVVSETGV- 173
D. vulgaris        GAEIVQD----------------------GLRID--GDPRAARDDIVGWAHDVRGAI--- 148
C. beijerinckii    GCVVVET------------------------PLIVQNEPDEAEQDCIEFGKKIANI---- 138
                   *                                :    :    .    :   .

YkuP long          CLITHWELLKRLFLFFLSLYLSFDTVMR 178
YkuP short         CAV------------------------- 151
YkuN               NKE--------------KIHVS------ 158
A. variabilis      ----------------------------
Synechococcus      ----------------------------
E. coli FldB       YA-------------------------- 173
E. coli FldA       EILNA----------------------- 175
C. crispus         ----------------------------
D. vulgaris        ----------------------------
C. beijerinckii    ----------------------------
```

FIGURE 3: Amino acid sequence alignment of *B. subtilis* YkuN and YkuP with other microbial flavodoxins. Alignment was generated using the ClustalW program via the EBI (http://www.ebi.ac.uk/clustalw/). The alignment uses both the YkuP sequence determined in this paper (YkuP short) and the sequence predicted from genome sequencing (YkuP long). These sequences are aligned with YkuN, the short-chain flavodoxins from *Desulfovibrio vulgaris* (*D. vulgaris*) and *Clostridium beijerinkii* (*C. beijerinkii*), and the long-chain flavodoxins from *E. coli* (*E. coli* FldA and *E. coli* FldB), *Anabaena variabilis* 7120 (*A. variabilis*), *Synechococcus* sp. PCC 7002 (*Synechococcus*), and *Chondrus crispus* (*C. crispus*). Residues indicated by asterisks are conserved in all sequences. Residues indicated by single and double dots are of similar and highly similar chemical character, respectively, according to criteria set in the program.

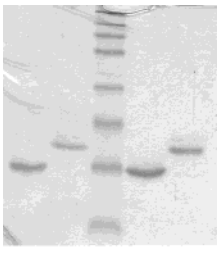

FIGURE 4: SDS−PAGE analysis of purified YkuN and YkuP. Purified YkuN (lanes 1 and 4, approximately 1 μg), YkuP (lanes 2 and 5, approximately 2 μg), and molecular weight markers (lane 3) are shown, resolved on a 15% SDS−PAGE gel. YkuP has lower electrophoretic mobility than YkuN. The broad range protein molecular weight markers shown (NEB) are of mass (top to bottom) 175, 83, 62, 47.5, 32.5, 25, 16.5, and 6.5 kDa. The flavodoxins migrate to positions between the 25 and 16.5 kDa markers.

removed). However, YkuP migrates more slowly on the SDS−PAGE gel with an estimated mass of ~20 kDa (cf. predicted mass of 16.7 kDa with methionine removed) (Figure 4). While the apparent mass difference between YkuN and YkuP likely reflects subtle structural alterations that impact electrophoretic mobility, we also sought confirmation of the short-chain flavodoxin nature of YkuN and YkuP by mass spectrometry (MALDI). The determined mass of YkuN (17 676 Da) is within 0.1% of that predicted on basis of the gene sequence. The determined mass of YkuP (16 527 Da) is within 1.3% of that predicted on the basis of our revised gene sequence (and clearly distinct from the 20 253 Da predicted from the published sequence). Thus, mass spectrometry is clearly supportive of our revised assignment of YkuP as a short-chain flavodoxin.

Spectral Properties of YkuN and YkuP. YkuN and YkuP were purified in their fully oxidized (quinone) forms. The UV−visible spectra of the oxidized flavodoxins show features typical of this class of flavin-binding proteins. Oxidized YkuN has two major absorption bands in the near-UV−visible region with maxima at 377.5 and 461.5 nm. There is a shoulder on the longer wavelength band at ~485

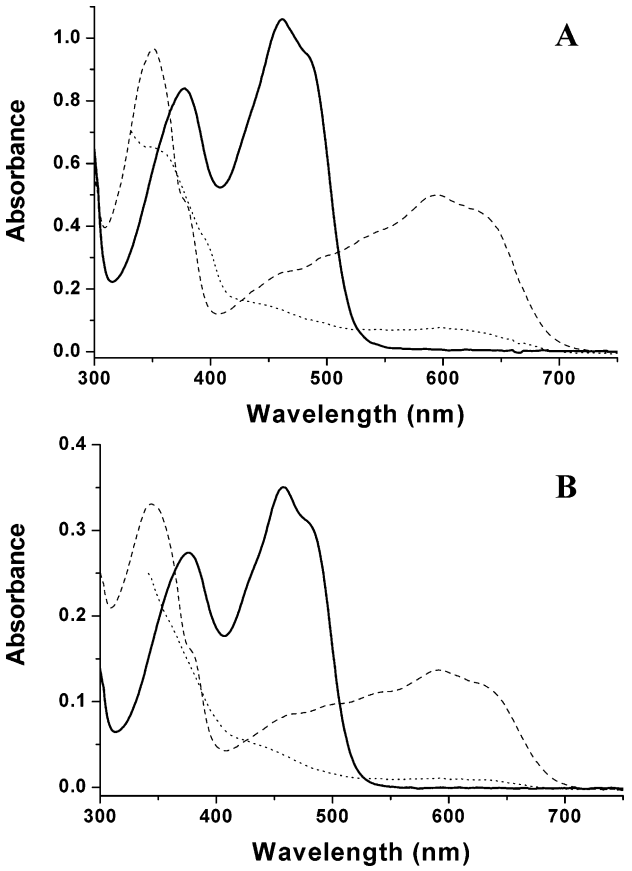

FIGURE 5: Spectral properties of YkuN and YkuP in their different redox states. Electronic absorption spectra for YkuN (panel A, ~100 μM) and YkuP (panel B, ~35 μM) are shown. Spectra are presented for the flavodoxins in their oxidized (—), semiquinone (···), and hydroquinone (– – –) forms. For the hydroquinone species, the spectra shown are those of the predominantly two-electron reduced forms of the flavodoxins, generated by addition of severalfold molar excess of sodium dithionite reductant.

nm (Figure 5A). YkuP has very similar characteristics with maxima at 377 and 457 nm and a shoulder at ~484 nm (Figure 5B). Highly purified YkuN was characterized with an A_{280}/A_{462} ratio of approximately 6:1 and YkuP with an A_{280}/A_{456} ratio of approximately 3.5:1. These ratio values are consistent with the higher content of aromatic amino acids in YkuN compared to YkuP, including two tryptophans in YkuN versus only one in YkuP (Figure 3). Partial reduction of both flavodoxins with the powerful reductant sodium dithionite produced species with spectral signatures characteristic of the neutral blue semiquinone state, that is, the form that is predominantly populated during expression of YkuN and YkuP in *E. coli*. These species exhibit a broad absorption band at long wavelength with a maximum at ~595 (YkuN) and ~592 nm (YkuP). A second sharp absorption feature is observed at 351 (YkuN) and 349 nm (YkuP). Independent evidence for the formation of the semiquinone species was obtained from electron paramagnetic resonance (EPR) analysis. The one-electron reduced forms of YkuN or YkuP produced EPR spectra characteristic for flavosemiquinones, showing a typical organic radical with a *g*-value of 2.007 for both YkuN and YkuP (not shown). Addition of excess dithionite results in the near-complete conversion of the flavodoxins to their two-electron reduced hydroquinone forms, in which absorption across the near UV−visible region is extensively bleached (Figure 5).

Reduction Potentials of the YkuN and YkuP Flavins. The capacity of both YkuN and YkuP to stabilize a one-electron reduced semiquinone species during reductive titrations enabled the accurate determination of the midpoint reduction potential of both the oxidized/semiquinone (ox/sq, E_1') and semiquinone/hydroquinone (sq/hq, E_2') couples. Potentiometric titrations were performed as done previously for *E. coli* FldA (*32*) and for other flavoproteins (*8*, *44*). Figure 6 shows the spectral titration data for YkuN (panels A and B) and for YkuP (panels C and D). Panels A and C show spectra collected during the first electron reduction of YkuN or YkuP, as the oxidized flavins are converted to their semiquinone forms. Panels B and D show spectra collected during the second electron reduction, as flavin semiquinones are converted to hydroquinone forms. Isosbestic points for the ox/sq transitions are located at ~510 and ~365 nm for YkuN and ~505 and ~364 nm for YkuP. Isosbestic points for the sq/hq transitions are located at ~429 and ~370 nm for YkuN and 425 and ~387 nm for YkuP. Figure 7 shows analysis of the spectral data with absorption versus potential plots presented at two different wavelengths. These wavelengths are (i) close to the semiquinone absorption maximum (596 nm for YkuN, 590 nm for YkuP; Figure 7A,B) and (ii) near the absorption maximum for the oxidized forms of the FMN (463 nm for YkuN, 459 nm for YkuP; Figure 7C,D). Data sets at both wavelengths were fitted to a two-electron Nernst function (eq 3) to define the midpoint reduction potentials (E_1' and E_2'). For YkuN, these analyses produce values of $E_1' = -105 \pm 3$, $E_2' = -382 \pm 5$ mV (at 596 nm) and $E_1' = -109 \pm 3$, $E_2' = -371 \pm 8$ mV (at 463 nm). For YkuP, the values are $E_1' = -105 \pm 4$, $E_2' = -377 \pm 4$ mV (at 590 nm) and $E_1' = -116 \pm 5$, $E_2' = -376 \pm 8$ mV (at 459 nm). The values determined at the different wavelengths are consistent with one another, and the large separations between the couples (~270 mV for both flavodoxins) are also consistent with the intensity of the blue semiquinone signal observed near 600 nm. The potentials obtained are compared with those determined previously for other flavodoxins in Table 1. Flavodoxins are often considered to cycle between hydroquinone and semiquinone forms as they pass electrons to redox partner enzymes (*30*). This model is certainly compatible with the relative potentials of the E_1 and E_2 couples in YkuN or YkuP and the midpoint reduction potential of the heme iron in fatty acid-bound P450 BioI (see accompanying manuscript, ref *36*). Electron transfer from the YkuN or YkuP hydroquinone ($E_2' \approx -375$ mV) to P450 BioI (≈ -200 mV) is strongly favored, whereas electron transfer from the semiquinone ($E_1' \approx -110$ mV) is clearly disfavored on thermodynamic grounds.

In parallel experiments, the reduction potentials of the YkuN or YkuP flavodoxins and P450 BioI were redetermined in a stoichiometric complex (as described in Experimental Procedures). The potentials for the oxidized/semiquinone and semiquinone/hydroquinone couples of YkuN were $E_1' = -111 \pm 8$ and $E_2' = -343 \pm 5$ mV and for YkuP $E_1' = -106 \pm 6$ and $E_2' = -378 \pm 10$ mV. These values are within error of those determined for the isolated flavodoxins (Table 1) with the exception of E_2' for the complexed YkuN, which is ~40 mV more positive than that for the isolated YkuN. This possibly reflects an altered environment of the YkuN FMN in the complex. Additionally, the potentials for the heme oxidized/reduced couple were -339 ± 5 mV in

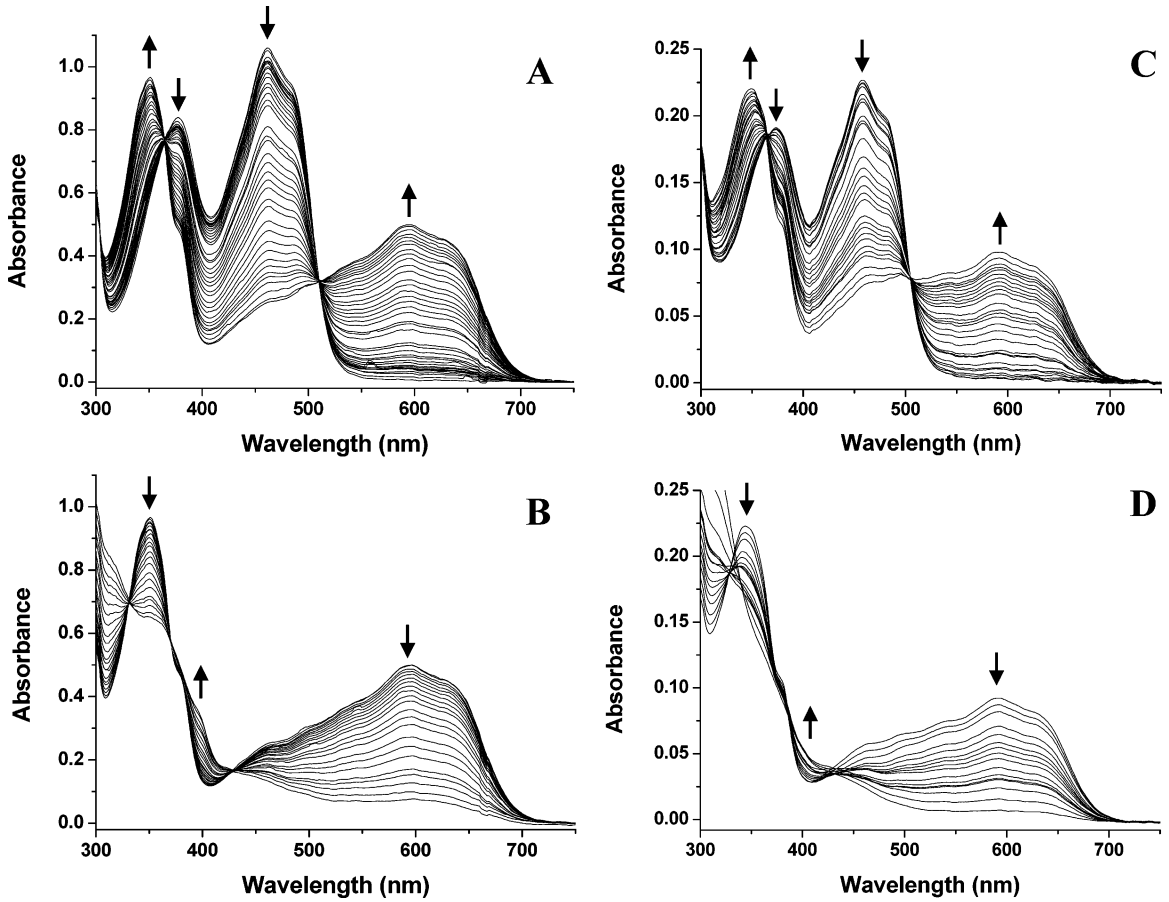

FIGURE 6: Spectrophotometric redox titrations of YkuN and YkuP. Selected absorption spectra accumulated during the potentiometric titration of YkuN (~100 μM, panels A and B) and YkuP (~21 μM, panels C and D) are shown. Panels A and C show spectra recorded during addition of the first electron (oxidized-to-semiquinone transition) to YkuN and YkuP, respectively. Panels B and D show spectra for the second electron reduction (semiquinone-to-hydroquinone transition) of YkuN and YkuP, respectively. Arrows indicate directions of absorption change at different wavelengths occurring in the reductive direction during the titrations.

the YkuN complex and -337 ± 5 mV in the YkuP complex. These values are rather more negative than those observed for the fatty acid-saturated (extensively high-spin) form of the P450 (≈ -200 mV, see ref *36*) and are more similar to those values for the substrate-free form of P450 BioI (≈ -330 mV). On complete reoxidation of the YkuN/BioI and YkuP/BioI complexes, the spectral maximum for the heme Soret band was seen to return to ~392 nm, indicating that the P450 remained in the fatty acid-bound, high-spin form when in its ferric form. Thus, the shift in heme potential may be a result of the influence of the binding of the flavodoxins close to the axial ligand of the heme iron. This being the case, the likelihood that electron transfer to the heme occurs from the YkuN or YkuP hydroquinone is reinforced.

Generation of YkuN and YkuP Apoproteins and Flavin-Binding Properties. The apoprotein forms of YkuN and YkuP were generated by TCA precipitation, as described in the Experimental Procedures section. Solubilized YkuN or YkuP apoproteins were devoid of the visible spectral properties typical of the holoflavodoxins, demonstrating that complete removal of the FMN cofactors had been achieved. To investigate the structural properties of the resolubilized apoflavodoxins, CD spectra in the far UV region (190−260 nm) were compared with those for the holoflavodoxins. In the case of YkuN, these CD spectra were almost indistinguishable, indicating that the conformation adopted by the apoprotein form is highly similar to that for the holoprotein (Figure 8A). However, the situation is different for YkuP. In the FMN-bound form, the CD spectrum is distinct from that for the YkuN holoflavodoxin (Figure 8B). There is a much stronger feature at ~210 nm for YkuP, suggesting differences in the relative proportions of the major secondary structural elements in the two holoflavodoxins. Specifically, the more intense feature in the YkuP spectrum might indicate a rather higher proportion of α helix. In the apoprotein form, the CD spectrum of YkuP is markedly distinct from that for the holoprotein (Figure 8B), suggesting that, unlike YkuN, a significant rearrangement of secondary structure occurs in the presence of the FMN cofactor.

The ability of both apoflavodoxins to bind FMN was confirmed by changes in the far-UV CD spectra (particularly obvious in the case of YkuP) indicative of a reversion to the holoprotein forms and by UV−visible absorption studies. The holoflavodoxins both exhibit a pronounced shoulder on their longer wavelength absorption band at approximately 485 (YkuN) and 484 nm (YkuP) (Figure 5). This feature is absent from free FMN but appears on titration of free FMN into the apoflavodoxins (not shown). To determine the apparent binding constants (K_d values) for the FMN cofactor, flavin fluorescence quenching experiments were performed using the apoflavodoxins, essentially as described in previous studies (*38*). Preliminary comparisons of the fluorescence of the FMN in YkuN and YkuP holoproteins demonstrated

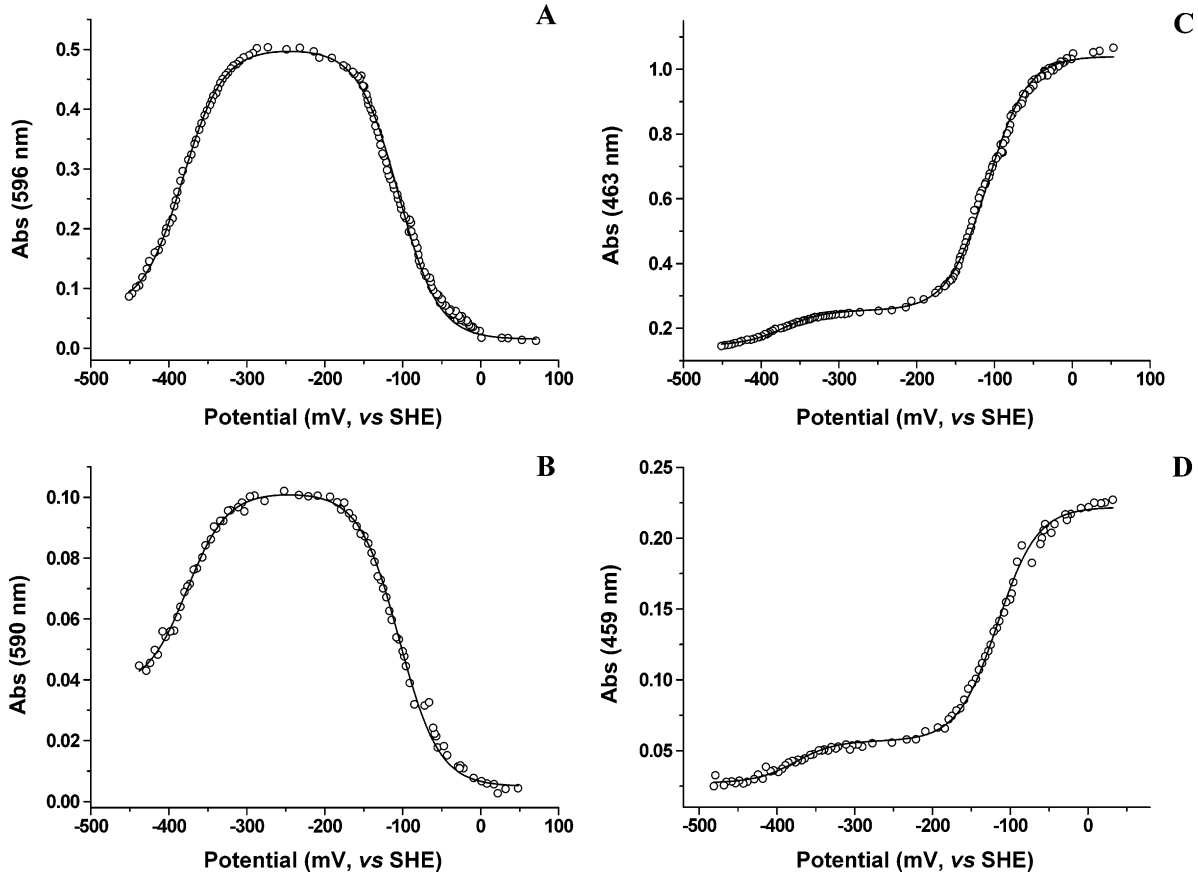

FIGURE 7: Analysis of potentiometric data for YkuN and YkuP. Absorption versus potential plots of redox titration data are shown with data fitted to eq 3. Panels A and B show data fits at 596 and 590 nm (near semiquinone maximum) for YkuN and YkuP, respectively. Panels C and D show data fits at 463 and 459 nm (near oxidized flavin maximum) for YkuN and YkuP, respectively. Data were collected and processed as described in the Experimental Procedures section. Resultant reduction potential values are collated in Table 1.

Table 1: Flavin Reduction Potentials in YkuN and YkuP[a]

		reduction potential (E', mV vs SHE)		
flavodoxin	species	E_1'	E_2'	E_{12}'
YkuN	*B. subtilis*	−105	−382	−244
YkuP	*B. subtilis*	−105	−377	−241
FldA	*E. coli*	−254	−433	−343
	A. nidulans	−221	−447	−334
	D. vulgaris	−143	−435	−285
	C. beijerinckii	−92	−399	−246
P450 BM3	*B. megaterium*	−213	−193	−203
CPR	*H. sapiens*	−43	−280	−162

[a] Midpoint reduction potentials for the oxidized/semiquinone (E_1'), semiquinone/hydroquinone (E_2'), and oxidized/hydroquinone (E_{12}') couples of the YkuN or YkuP flavodoxins were determined as described in the Experimental Procedures section. Values are compared with those for long-chain flavodoxins from *E. coli* (FldA, ref *32*) and *Synechococcus* PCC 6301 (*Anacystis nidulans*, ref *59*) and with those for short-chain flavodoxins from *D. vulgaris* (*49*) and *C. beijerinckii* (*55*). Also included are the reduction potential values for the FMN-containing (flavodoxin-like) domains of P450 reductase enzyme from *B. megaterium* (CYP102A1, P450 BM3, ref *41*) and human (P450 reductase, CPR, ref *8*). All values reported were determined at pH 7.0. Values cited for the *B. subtilis* flavodoxins are from analysis of absorption versus potential data at wavelengths near-maximal for the semiquinone species.

that it was considerably quenched (1.5% and 0.4% of that for free FMN) by the protein. As expected, saturable quenching of FMN fluorescence was observed on progressive titration of a solution of FMN with both apoYkuN and apoYkuP. Plots of the flavin fluorescence change against the concentration of apoflavodoxin added were fitted to eq 2 to yield apparent K_d values of 14.6 ± 0.6 nM for YkuN and 25.2 ± 1.0 nM for YkuP for FMN binding. These values reflect very tight binding of FMN for the apoflavodoxins but are slightly weaker than K_d values determined for certain other bacterial flavodoxins (e.g., that from *D. vulgaris* at ∼2.4 nM, ref *45*). However, these K_d values are similar to that determined for the *Cl. beijerinkii* flavodoxin (∼18 nM, ref *46*) under similar conditions. It should be noted, however, that phosphate ions may compete at the FMN binding site and that effects may vary according to the particular flavodoxin studied (*45*). Importantly, negligible quenching of riboflavin fluorescence was observed with either apoYkuN or apoYkuP. These findings are consistent with the properties of "typical" short-chain flavodoxins, which have a rather strict requirement for the terminal phosphate of FMN. In turn, this provides yet further evidence that YkuP is a member of this broad class of short-chain flavodoxins (*47*, *48*). However, a notable exception to this "rule" is the short-chain flavodoxin from *D. vulgaris*, which does bind riboflavin, albeit ∼3000-fold more weakly than it does FMN (*49*). In structural studies of the riboflavin-bound *D. vulgaris* flavodoxin, sulfate or phosphate ions from the crystallization buffer were found to occupy the structural space that would be occupied by the 5′-phosphate of FMN in the native flavodoxin (*47*).

Structural Stability of YkuN and YkuP. Flavodoxins are typically robust proteins, requiring high concentrations of chaotropes to induce complete unfolding and cofactor loss (e.g., refs *32* and *50*). In view of the apparent structural

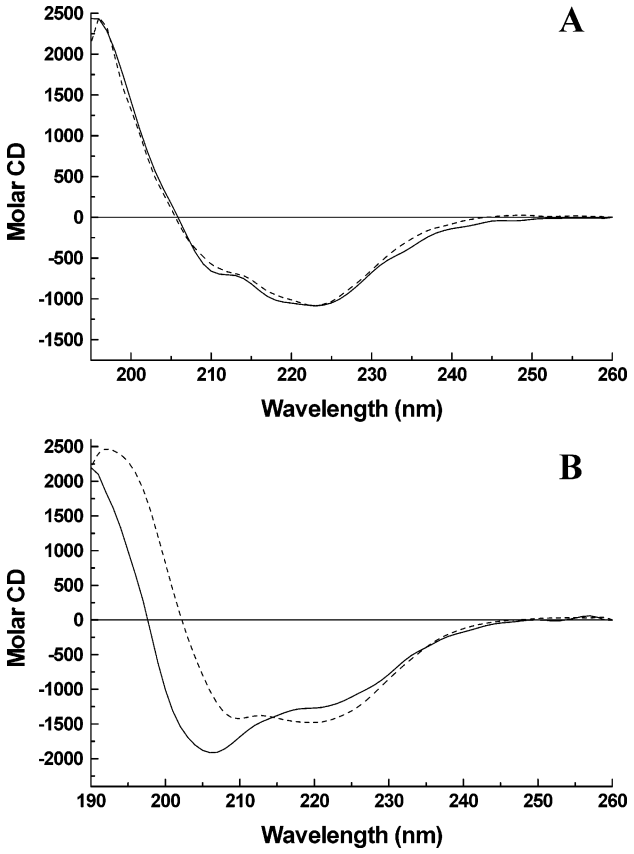

FIGURE 8: CD spectra for holoprotein and apoprotein forms of YkuN and YkuP. Far-UV CD spectra were collected for both holo- and apo-forms of YkuN and YkuP, as described in the Experimental Procedures section. Panel A shows CD spectra for the YkuN holoprotein (—) and apoprotein (– – –). Panel B shows CD spectra for the YkuP holoprotein (– – –) and apoprotein (—).

differences between YkuN and YkuP evident from their distinctive CD properties in holo- and apo-forms, and in light of the slightly weaker binding of FMN compared to certain other bacterial flavodoxins, we undertook studies on the stability of structure and flavin binding in YkuN and YkuP. This was done both by examining the effects of guanidinium chloride (GdmCl) on secondary structure, tertiary structure, and flavin binding and by evaluating the thermodynamic parameters associated with thermal unfolding of the flavodoxins using differential scanning calorimetry (DSC).

Structural Stability of YkuN and YkuP: GdmCl-Induced Unfolding. Preliminary studies involved the examination of the dissociation of FMN cofactor from its active site in YkuN or YkuP by following the change in electronic absorption spectrum of the flavodoxins at different concentrations of GdmCl. As GdmCl concentration was increased, similar perturbations in the optical spectra of both YkuN and YkuP were observed. At high GdmCl concentration, the position of the first (shorter wavelength) visible absorption band shifted by only ~1 nm (from ~377 to ~378 nm with slight increase in intensity), but the spectral maximum for the longer wavelength band was blue-shifted to approximately 448 nm (from 461.5 or 457 nm for YkuN or YkuP), and the pronounced shoulder associated with the flavodoxin-bound form of FMN was lost. The spectrum of free FMN has maxima at approximately 374 and 446 nm in GdmCl-free buffer, shifting to 378 and 448 nm in 8 M GdmCl. This indicates that FMN is stoichiometrically dissociated from the YkuN or YkuP protein matrixes at high GdmCl concentration. Plots of the GdmCl-induced absorption changes versus GdmCl concentration described sigmoids and were fitted to the Hill equation to produce midpoint values for GdmCl-induced flavin loss of 1.99 ± 0.1 M for YkuN and 1.10 ± 0.04 M for YkuP.

The effects of GdmCl on fluorescence from aromatic amino acids (primarily tryptophan) were examined to provide further information on stability of tertiary structure. Previous titrations of apoflavodoxins with FMN showed clearly that quenching of flavin fluorescence was associated with binding of FMN to the proteins. Treatment of YkuN and YkuP with GdmCl resulted in increased tryptophan fluorescence and a shift in the fluorescence emission λ_{max} from 348 to 360 nm (YkuN) and from 352 to 362 nm (YkuP). Data plots for change in fluorescence versus GdmCl concentration were again sigmoidal and produced midpoint values of 2.45 ± 0.18 (YkuN) and 1.90 ± 0.51 M (YkuP). The stability measurements were repeated using the apoflavodoxin forms, generated by TCA precipitation as described in the Experimental Procedures section. In these cases, the results were rather different. In the case of YkuN, the emission λ_{max} for protein without GdmCl added was at 350 nm and shifted to 359 nm at the end point in the titration with the chaotrope. The slightly shifted λ_{max} in the GdmCl-free form (350 nm; cf. 348 nm in holo-YkuN) likely reflects greater solvent accessibility of the tryptophan residues in the apo-YkuN. One of the two tryptophan residues in YkuN is Trp60, located in the FMN-binding loop region, and is likely affected by displacement of the flavin (Figure 3). The midpoint value for GdmCl-induced fluorescence change in apo-YkuN was 1.71 ± 0.10 M, suggesting moderate destabilization of the tertiary structure of the apoprotein with respect to the holoflavodoxin. Interestingly, the behavior of apo-YkuP is rather different. In the apo-form, the λ_{max} for fluorescence emission is located at 348 nm, rather than at 352 nm as in the holo-form, possibly indicating that the single tryptophan in this isoform (Trp60) adopts a more buried, hydrophobic environment in the absence of FMN. The midpoint value for GdmCl-induced fluorescence change in apo-YkuP was 3.13 ± 0.24 M, suggesting greater stability of tertiary structure than that of the holoprotein (1.90 ± 0.51 M). This marked apparent change in stability of tertiary structure in the apo-form of YkuP may reflect the notable change in secondary structure observed in CD studies (Figure 8B).

Previous titrations of apoflavodoxins with FMN showed clearly that quenching of flavin fluorescence was associated with binding of FMN to the proteins. To investigate the stability of FMN binding, studies of the change in flavin fluorescence at different concentrations of GdmCl were performed. Intensity of flavin fluorescence increased as GdmCl concentration was elevated. However, it was found that, for both YkuN and YkuP, the λ_{max} for fluorescence of GdmCl-free holoprotein was located at ~528 nm (with excitation at 450 nm) and that the wavelength of maximum emission did not change to any significant extent at different concentrations of GdmCl. This may reflect the superficial positioning of the isoalloxazine ring of the FMN in the protein structures and that the polarity of its environment is not changed greatly as it is released into the solvent at high GdmCl concentration. For YkuN, the flavin fluorescence changes again showed a sigmoidal dependence on GdmCl

Table 2: Structural Stability of YkuN and YkuP to the Chaotrope Guanidinium Chloride[a]

	midpoint stability to GdmCl (K^U,M)			
	YkuN		YkuP	
	holoprotein	apoprotein	holoprotein	apoprotein
far-UV CD	2.92 ± 0.04	2.18 ± 0.11	2.30 ± 0.19	2.50 ± 0.16
flavin fluorescence	1.95 ± 0.14		0.99 ± 0.20	
tryptophan fluorescence	2.45 ± 0.18	1.70 ± 0.10	1.90 ± 0.51	3.13 ± 0.24
flavin binding	1.99 ± 0.1		1.10 ± 0.04	

[a] The table shows the midpoint concentrations (K^U values) of guanidinium chloride (GdmCl) required for (a) loss of secondary structure (by far-UV CD), (b) flavin dissociation (by flavin fluorescence), (c) loss of tertiary structure (by tryptophan fluorescence), and (d) flavin loss or disruption of flavin binding (by electronic absorption spectroscopy). Data were collected and processed as described in the Experimental Procedures section.

concentration with a midpoint value of 1.95 ± 0.14 M, very similar to the midpoint value for GdmCl-induced flavin absorption change (1.99 ± 0.10 M). YkuP flavin fluorescence increase at 528 nm also showed a sigmoidal dependence on GdmCl concentration at rather lower concentrations of the chaotrope with a midpoint value of 0.99 ± 0.20 M, again consistent with the value determined from flavin absorption changes (1.10 ± 0.04). The rather lower stability of flavin binding in YkuP is consistent with the observation that some FMN is lost from this protein (but not YkuN) following extended protein concentration by ultrafiltration.

To investigate stability of secondary structure to GdmCl-induced denaturation, CD spectra in the far-UV region (190−260 nm) were recorded for both holo- and apo-forms of YkuN and YkuP across a GdmCl concentration range (0−8 M). Induced change in secondary structure (represented by change in CD signal at 222 nm) was plotted versus the relevant GdmCl concentration, again displaying an apparently sigmoidal dependence of CD change on chaotrope concentration. The midpoint GdmCl concentration values for secondary structure loss were 2.92 ± 0.04 and 2.18 ± 0.11 for YkuN holoprotein and apoprotein, respectively, and 2.30 ± 0.19 and 2.50 ± 0.16 M for YkuP. The results indicate that there is moderate destabilization of the secondary structure on removal of the FMN from YkuN but that YkuP is largely unaffected (or even slightly stabilized) by FMN removal. All numerical data from the chaotrope stability studies are presented in Table 2.

Structural Stability of YkuN and YkuP: Differential Scanning Calorimetry (DSC) Studies. Figure 9 shows the results of DSC scans conducted with native YkuN and YkuP. During initial heating scans, the experiments were terminated shortly after the T_m had been reached. The proteins were allowed to cool to room temperature, and then they were rescanned. The results indicated that unfolding of these flavodoxins is largely reversible. However there is a small degree of hysteresis and during the rescan; about 10% of the transition is lost. The data shown in Figure 9 are initial scans that were collected beyond the T_m so that adequate post-transition baselines were collected for data analysis. After subtraction of the buffer baseline, linear least-squares fits to the pre- and post-transitional baselines for YkuN were used to determine the heat capacity change for unfolding of this protein. A similar procedure could not be conducted on YkuP since the post-transitional baseline became slightly exothermic in all cases, probably due to slight aggregation. Baseline-corrected data for both proteins were best fitted using a non-two-state model. The most notable difference in the two proteins is that the DSC endotherm for YkuN (panel A in Figure 9) is clearly biphasic, and these data were best fitted to two-component transitions. Conversely, the DSC endotherm for YkuP was composed of a single transition. The calorimetrically derived thermodynamic parameters for the unfolding of these proteins are collated in Table 3.

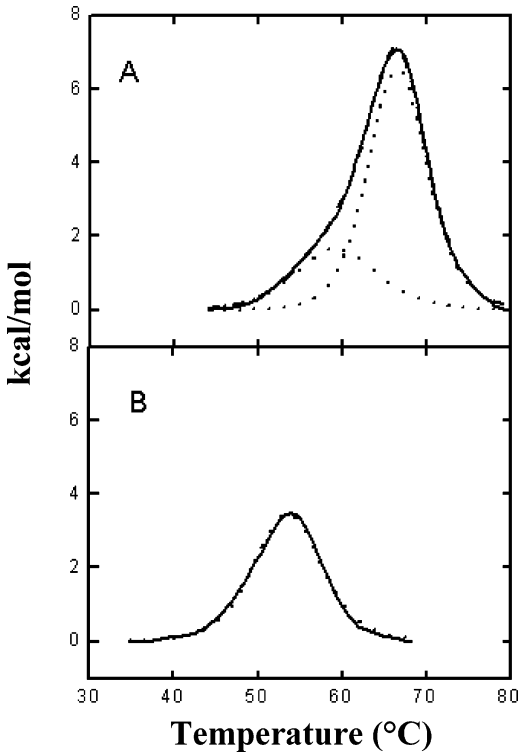

FIGURE 9: DSC analysis of the YkuN and YkuP flavodoxins. DSC scans for the *B. subtilis* flavodoxins YkuN (panel A) and YkuP (panel B) are shown. In both scans the solid lines are experimentally measured unfolding endotherms, and the dotted lines are nonlinear least-squares best fits to the data obtained using a non-two-state unfolding model incorporated in Origin 7.0. Data were collected as described in the Experimental Procedures section.

Table 3: Calorimetrically Derived Thermodynamic Parameters for the Unfolding of YkuN and YkuP[a]

protein	T_m (°C)	ΔH_{cal} (kcal mol^{-1})	ΔH_{vH} (kcal mol^{-1})	ΔC_p (kcal mol^{-1} K^{-1})	$\Delta H_{vH}/\Delta H_{cal}$
YkuN				+870 (total)	
trans. 1	59.5	24	64		2.7
trans. 2	66.7	58	101		1.7
YkuP	53.5	42	74	ND	1.7

[a] The parameters derived from DSC studies on the holoflavodoxins YkuN and YkuP are shown. Data were collected as described in the Experimental Procedures section. Heat capacity change (ΔC_p) was calculated for YkuN from a linear least-squares fit to pre- and post-translational baseline data, following subtraction of the buffer baseline. The same procedure was not possible for YkuP (ND = not determined), since the post-transitional baseline was slightly exothermic in all experiments, probably due to some YkuP aggregation.

Straightforward analysis of DSC data relies on the thermal transitions being reversible and being under thermodynamic rather than kinetic control. For the two proteins under study here, repeat scans showed that unfolding was largely

reversible and hence equilibrium thermodynamics can be used to analyze the data. This was done to determine both calorimetric (ΔH_{cal}) and van't Hoff (ΔH_{vH}) enthalpies. The former is obtained directly from the experimental data by simple integration, and the latter comes from nonlinear least-squares fits to the data and the line shape. These are useful parameters since their ratio yields information about the cooperativity of unfolding. If unfolding is perfectly two-state, then ΔH_{cal} should equal ΔH_{vH}. However examination of Table 3 indicates that for both proteins the van't Hoff enthalpy is always larger than the calorimetric enthalpy. This is normally an indication of aggregation. This is consistent with the small degree of hysteresis observed and exothermic posttransitional baselines for YkuP.

It is clear from both Figure 9 and Table 3 that YkuP is thermodynamically less stable than YkuN. It has a lower T_m and a much smaller ΔH_{cal}. It also unfolds in essentially a two-state manner compared to the more complex thermal unfolding of YkuN. A heat capacity change could not be measured for YkuP for reasons mentioned above. However for YkuN the ΔC_p for unfolding is typical for a protein of this size and results from the exposure of hydrophobic residues to water. The differences in DSC data for YkuN and YkuP are generally consistent with the data from CD studies (which indicate structural differences between the holoflavodoxins) and with data from FMN binding and GdmCl denaturation studies, which indicate that YkuP binds more weakly to FMN and has lower tertiary and secondary structural stability.

Spectroscopic and Kinetic Interactions of YkuN and YkuP with P450 BioI and NADPH−Flavodoxin Reductase: Static Absorption and Fluorescence Titrations. A key reason for expressing and characterizing the *B. subtilis* flavodoxin proteins was to analyze their interactions with the host P450 BioI system (see accompanying paper, ref *36*) and to establish the efficiency of their redox reactions with this enzyme. In preliminary optical titration studies, small perturbations of the heme iron spin-state of the substrate-free P450 BioI enzyme (toward the high-spin form) were observed on addition of the flavodoxins. While these absorption changes were relatively small compared to those observed on binding of fatty acids to the P450 (see accompanying paper, ref *36*), plots of the changes in heme absorption induced (A_{394} minus A_{413}, reflecting the wavelengths showing the maximal overall change in absorption) versus flavodoxin concentration described hyperbolae. These were fitted to eq 1 to yield apparent K_d values of 1.93 ± 0.15 μM for YkuN and 4.98 ± 1.67 μM for YkuP. These values compare well with the binding constant for the *B. subtilis* ferredoxin (Fer) to P450 BioI (K_d = 0.87 ± 0.10 μM) (17). Similarly, in fluorimetric titrations, quenching of flavin fluorescence (measured at 528 nm) was observed on titration of substrate-free P450 BioI (0.7 μM) with oxidized YkuN or YkuP. While apparent flavin fluorescence change did not follow a hyperbolic dependence on the concentration of YkuN or YkuP added (preventing accurate determination of K_d values), tight interactions between the proteins were evident. In the case of YkuN, the fluorescence change was complete by the point that ~0.8 μM flavodoxin was added, indicating the K_d should be ≤0.4 μM. Similarly, the titration with YkuP was complete by the point of addition of ~1.7 μM, indicating the K_d should be ≤0.85 μM. By both methods, there is an approximately 2-fold higher affinity for P450 BioI with oxidized YkuN over oxidized YkuP.

Spectroscopic and Kinetic Interactions of YkuN and YkuP with P450 BioI and NADPH−Flavodoxin Reductase: Transient Kinetic Studies. To define the kinetics of the reactions relating to YkuN or YkuP and the P450 BioI redox system, a series of stopped-flow investigations were performed. The electron-transfer reactions between the flavodoxins and P450 BioI, and between the flavodoxins and a prototypical flavodoxin reductase (*E. coli* NADPH−flavodoxin/ferredoxin oxidoreductase, FLDR, ref *32*) were investigated.

To determine the rate of electron transfer between reduced YkuN or YkuP and P450 BioI, stopped-flow mixing of the reduced (hydroquinone) forms of the flavodoxins with substrate (palmitoleic acid)-bound and testosterone-bound forms of P450 BioI was performed, as described in the Experimental Procedures section. In the palmitoleate-bound form, the P450 BioI heme iron is in an extensively high-spin form and has a less negative reduction potential, and reduction of the heme iron by the flavodoxins should be more thermodynamically favorable. In the testosterone-bound form, the heme iron is low-spin, the potential is more negative, and electron transfer should be less favorable. The stopped-flow experiments were done in an anaerobic glovebox in carbon monoxide (CO)-saturated buffer. This results in the rapid binding of CO to the ferrous heme iron following electron transfer from the flavodoxins and the development of the UV−visible spectrum characteristic for a CO-bound P450 with Soret absorption maximum close to 450 nm (448 nm in the case of P450 BioI). Figure 10A shows spectral data accumulated using the photodiode array attachment on the stopped-flow instrument for the reaction of reduced YkuN with fatty acid-bound P450 BioI. The predominant spectral change observed is the shift of the BioI Soret band to 448 nm as the ferrous CO complex forms. In single-wavelength mode (i.e., monitoring the ΔA_{448}), absorption transients were collected across a range of concentrations of YkuN and YkuP at a fixed concentration of palmitoleate-bound and testosterone-bound P450 BioI. The absorption transients fitted well to a single-exponential function, and the reaction rate versus flavodoxin concentration data were fitted to eq 1 to determine apparent limiting electron-transfer rate constants (k_{red}) for heme reduction and to determine apparent K_d values for the flavodoxin/P450 BioI interactions. Under the same conditions, heme reduction of palmitoleate-bound BioI was also analyzed using *E. coli* flavodoxin (FldA) and spinach ferredoxin. The data resulting from these experiments are shown in Table 4. A typical graph showing the dependence of heme iron reduction rate for palmitoleate-bound BioI with reduced YkuP is shown in Figure 10B. The data show that both YkuN and YkuP are more efficient in first electron transfer to the substrate-bound P450 BioI than are the spinach ferredoxin or *E. coli* FldA with k_{red} values ~2.6−2.9-fold faster than the spinach ferredoxin and 12.5−13.9-fold faster than FldA (Table 4). Apparent K_d values are relatively similar for all of the flavodoxins/ferredoxin. The k_{red} values for YkuN- or YkuP-dependent heme reduction in the testosterone-bound forms are, as expected, considerably (>10-fold) slower than those for the substrate-bound P450s. Interestingly, the apparent K_d value for YkuP determined from analysis of reduction of testosterone-bound BioI is markedly lower than for the palmitoleate-bound enzyme. This could

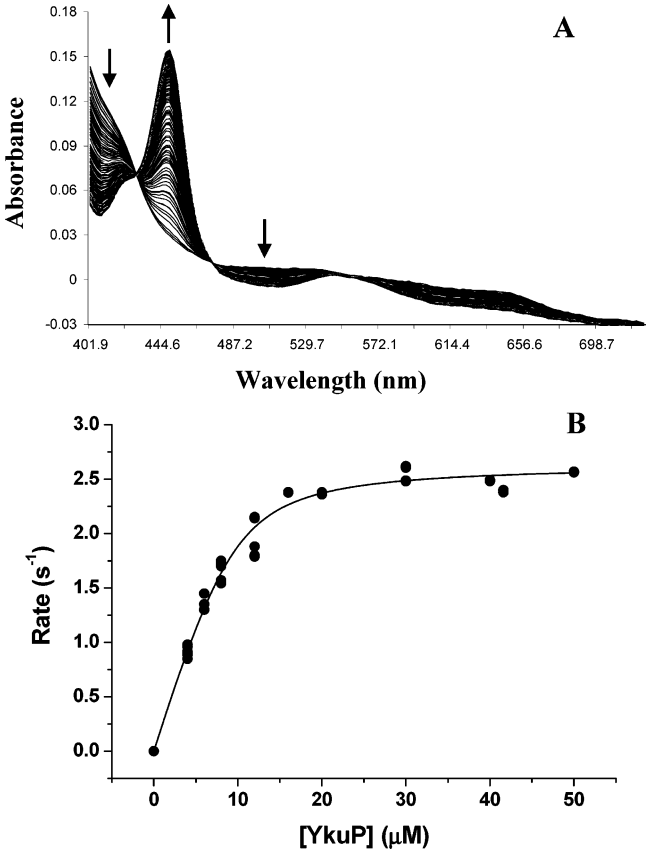

FIGURE 10: Electron transfer from YkuN and YkuP to P450 BioI. Panel A shows photodiode array spectral data for the reduction of substrate (palmitoleate)-bound P450 BioI (1.8 μM) by YkuN (30 μM), as described in the Experimental Procedures section. Arrows indicate direction of absorption change as the P450 is converted to its ferrous−CO adduct. Panel B shows a plot of apparent palmitoleate-bound P450 BioI reduction rate versus concentration of the flavodoxin (YkuP). Data are fitted to eq 1 to yield parameters of limiting heme iron reduction rate (k_{red}) = 2.64 ± 0.05 s^{-1} and apparent binding constant (K_d) = 1.30 ± 0.33 μM.

Table 4: Reduction of P450 BioI by Flavodoxin and Ferredoxin Redox Partners[a]

redox partner protein	molecule bound			
	palmitoleic acid		testosterone	
	k_{red} (s^{-1})	K_d (μM)	k_{red} (s^{-1})	K_d (μM)
YkuN	2.38 ± 0.05	0.32 ± 0.13	0.19 ± 0.01	0.54 ± 0.17
YkuP	2.64 ± 0.05	1.30 ± 0.33	0.29 ± 0.01	0.63 ± 0.31
spinach Fd	0.92 ± 0.02	0.24 ± 0.09	*b*	*b*
E. coli FldA	0.19 ± 0.01	2.10 ± 0.25	*b*	*b*

[a] The heme iron reduction rates were measured for palmitoleate-bound (high-spin) P450 BioI as described in the Experimental Procedures section. Limiting reduction rates (k_{red}) and apparent binding constants (K_d values) are given for the reductive reactions with *B. subtilis* flavodoxins YkuN and YkuP, *E. coli* flavodoxin (FldA), and spinach ferredoxin (spinach Fd). The kinetic parameters are compared with those for reduction of the testosterone (inhibitor)-bound, low-spin P450 BioI by YkuN and YkuP. [b] Not determined.

obviously reflect P450 conformational changes accompanying either testosterone binding or spin-state change that impact on the binding sites of the YkuP flavodoxin (Table 4).

To determine the kinetics of interactions between *E. coli* flavodoxin reductase (FLDR) and the *B. subtilis* flavodoxins, a further series of stopped-flow experiments were performed in which NADPH-reduced FLDR (various concentrations) was mixed with oxidized YkuN and YkuP (single, fixed concentration), and the electron-transfer rate was measured as a function of the absorption increase at 591 nm, specific for the development of the neutral blue semiquinone species, as described in the Experimental Procedures section. The flavodoxins stabilize the blue semiquinone species (Figure 5) but the FLDR does not in equilibrium titrations (*32*). Any semiquinone formation on the FLDR during the reactions is expected to occur concomitantly with that on YkuN and YkuP. In agreement with this hypothesis, reaction transients at 591 nm were monophasic and were fitted to a single-exponential function. Reaction rate versus FLDR concentration data were plotted and fitted to eq 1 to yield parameters of k_{red} (apparent interflavin electron-transfer limiting rate constant) = 3.75 ± 0.12 (YkuN) and 3.05 ± 0.15 s^{-1} (YkuP) and K_d = 16.2 ± 1.7 (YkuN) and 10.6 ± 1.6 μM (YkuP).

Table 5: Steady-State Turnover Rates for P450 BioI with YkuN and YkuP as Redox Partners[a]

P450 BioI substrate	redox partner and kinetic parameters			
	YkuN		YkuP	
	k_{cat} (min^{-1})	K_M (μM)	k_{cat} (min^{-1})	K_M (μM)
palmitoleate	25.7 ± 1.5	11.5 ± 1.5	23.9 ± 1.0	14.7 ± 1.4
palmitate	72.3 ± 1.8	5.3 ± 0.6	88.9 ± 4.7	18.0 ± 2.4
myristate	75.3 ± 2.6	6.7 ± 0.9	82.9 ± 3.5	20.8 ± 2.2
laurate	81.5 ± 2.9	6.0 ± 0.9	103.9 ± 5.2	15.8 ± 2.2

[a] The steady-state turnover of palmitoleic acid (palmitoleate), palmitic acid (palmitate), myristic acid (myristate), and lauric acid (laurate) was analyzed as described in the Experimental Procedures section. The apparent k_{cat} and K_M values for the YkuN and YkuP flavodoxins were determined by varying concentration of the flavodoxins while maintaining the concentration of P450 BioI constant in assays.

Spectroscopic and Kinetic Interactions of YkuN and YkuP with P450 BioI and NADPH−Flavodoxin Reductase: Steady-State Kinetics. To analyze the apparent turnover rates of systems containing NADPH, FLDR, YkuN or YkuP, and substrate-bound P450 BioI, steady-state studies were performed as described in the Experimental Procedures section. At fixed concentrations of FLDR, P450 BioI, fatty acid substrate, and NADPH, the oxidation of NADPH (ϵ_{340} = 6.21 mM^{-1} cm^{-1}) was measured across a range of concentrations of YkuN or YkuP. In this way, apparent K_m values for the flavodoxins could be determined, along with the apparent k_{cat} values for the systems, expressed as moles of NADPH oxidized per minute per mole of P450. In preliminary experiments, the palmitoleic acid-induced oxidation of NADPH was compared between systems in which either YkuN, YkuP, or *E. coli* FLD were used to mediate electron transfer between FLDR and P450 BioI. In these systems, the apparent k_{cat} values for YkuN and YkuP were similar (25.7 ± 1.5 and 23.9 ± 1.0 min^{-1}, respectively), but there was neglible (<1 min^{-1}) turnover with the *E. coli* FldA. The kinetic parameters (apparent k_{cat} and K_m for flavodoxin) for turnover of palmitoleic acid, lauric acid, myristic acid, and palmitic acids with YkuN and YkuP are shown in Table 5. These data indicate that turnover rates of up to ~100 min^{-1} are feasible with both YkuN and YkuP and the saturated fatty acids, and that the affinity for YkuN is generally 2−3-fold higher than that for YkuP. The magnitudes of the apparent rate constants suggest that interflavin and flavin-to-heme electron transfer reactions should be major contributory factors to rate limitation in these systems. This would

also be consistent with the relatively slow rate of electron transfer between *E. coli* FldA and the BioI heme iron determined in stopped-flow studies and with the slow rate of FLDR-to-FldA electron transfer reported previously (*32*). Electron transfer between putidaredoxin and the P450 (as opposed to, for example, substrate binding or release steps) is considered to be rate-limiting in turnover of the well-studied P450 cam system from *P. putida* (*51*).

Analysis of Fatty Acid Oxidation in Turnover Systems Containing YkuN or YkuP and P450 BioI. In preliminary studies to examine production of oxygenated lipid products, the effects of various parameters (including redox partner [P450, FLDR, YkuN or YkuP] concentrations, pH, and reaction volume) were investigated to establish conditions optimal for best production of oxygenated myristic acid. The major factors promoting high levels of product yield were found to be high concentrations of P450 BioI and NADPH. Product formation was followed using electrospray mass spectrometry, as described in the Experimental Procedures section. Under optimal conditions using YkuN, approximately 74% of myristic acid was converted to a monohydroxylated product by P450 BioI. Under the same conditions, ~37% of myristic acid was similarly converted to monohydroxylated product with YkuP as the redox partner. Given the superior level of turnover achieved with the YkuN flavodoxin, further studies of YkuN-supported fatty acid oxygenation were performed using lauric acid, 13-methyl myristic acid (a branched chain fatty acid present in *B. subtilis* membranes), palmitic acid, and the monounsaturated palmitoleic acid. Approximately 55% of the lauric acid was converted to monohydroxylated product. However, there was only ~3% conversion of 13-methyl myristic acid to a monohydroxylated product under the same conditions. While palmitoleic acid and palmitic acid were not oxygenated as efficiently as lauric acid and myristic acid, there was clear evidence for the production of both mono- and dihydroxylated forms of both palmitate (5.5% and 2.2%, respectively) and palmitoleate (3.0% and 4.0%, respectively). No formation of oxygenated product was observed after extended incubations with testosterone. In parallel control studies, only a small amount of peroxide (<1% of the amount of NADPH oxidized) was produced during turnover of the various fatty acid substrates (37). However, since there is clearly not complete coupling of NADPH oxidation to fatty acid oxygenation in these systems (see data above), electrons must also be diverted to superoxide and or water formation. Potentially, more efficient turnover may occur in the presence of a *B. subtilis* reductase.

The results show clearly that both YkuN and YkuP are capable of supporting fatty acid oxygenation catalyzed by P450 BioI. These results are consistent with previous studies using the *B. subtilis* ferredoxin Fer as the redox partner (*16*) and with the flavodoxin (cindoxin) from *C. braakii* (*21*). In recent studies, De Voss and co-workers have characterized the regioselectvity of hydroxylation of myristic acid (showing hydroxylation at ω-1, ω-2, and ω-3 positions with the ω-3 hydroxy product predominant) and of palmitic acid (hydroxylation at positions from ω-1 through ω-5 in roughly similar proportions) (*22*). In their study, only monohydroxylated products were observed under non-steady-state turnover conditions (4.8 μM P450 BioI reacted with 2.4 μM fatty acid). However, evidence presented here is that at least palmitic acid and palmitoleic acid can be oxygenated twice with the monohydroxylated product acting as substrate for a second round of oxygenation. Such behavior has been observed in the *B. megaterium* P450 BM3 fatty acid hydroxylase (*50*).

DISCUSSION

The *B. subtilis* genome sequence indicated the presence of two genes encoding putative flavodoxin-like proteins (*20*). In this paper, we have expressed the *ykuN* and *ykuP* genes and demonstrated that both encoded proteins are FMN-binding flavodoxins and have characterized their kinetic, spectroscopic, biophysical, and thermodynamic properties. DNA sequencing of several clones of *ykuP* revealed a single nucleotide difference from the published sequence. This difference has an important impact on the classification of the YkuP flavodoxin. According to the published genome sequence, YkuP was predicted to be larger than YkuN (20.3 kDa, cf. 17.8 kDa) and thus to be a member of the long-chain flavodoxin subclass of proteins (whereas YkuN is a short-chain flavodoxin). SDS−PAGE analysis (Figure 4) would be supportive of this assignment, since YkuP has lower electrophoretic mobility than YkuN under denaturing conditions. However, our resequencing of *ykuP* indicates that the reading frame is altered in the latter part of the gene and that a stop codon is encountered earlier than would be the case from genome sequence data. This results in the predicted mass of YkuP being only 16.9 kDa and its reclassification as a short-chain flavodoxin. Amino acid sequence alignment data (Figure 3) indicate strongly that this should be the case. The additional YkuP amino acids predicted on the basis of genome sequencing are not recognized as forming an "insert" region seen intervening the final beta strand segment of the long-chain flavodoxins. Instead, the alignment places them at the end of the protein and not aligning with any regions from the other flavodoxins. In contrast, the amino sequence generated from our resequencing predicts a typical short-chain flavodoxin, which aligns well with other flavodoxin sequences. Additional confirmatory data supporting the reclassification of YkuP as a short-chain flavodoxin comes from mass spectrometry and from the fact that neither YkuN nor YkuP have measurable affinity for riboflavin from fluorescence quenching experiments.

Intriguing differences are noted between the general structural features and stabilities of YkuN and YkuP. The secondary structure (by far-UV CD) of YkuN holoprotein and apoprotein are highly similar (Figure 8), indicating that FMN-binding does not have a significant effect on folding of the protein. In contrast, the apoprotein and holoprotein forms of YkuP are significantly different, indicating that binding of FMN impacts considerably on the final conformation of YkuP. The stability of holo-YkuN flavin binding and secondary and tertiary structure to disruption by guanidinium chloride is consistently greater than that of holo-YkuP. These data are in agreement with the results from DSC analysis, which indicate lower thermal stability for YkuP (Table 3). Further evidence for the conformational differences between the apo- and holo-forms of YkuP are that removal of FMN destabilized secondary and tertiary structure in YkuN but that the apoprotein form of YkuP is actually somewhat more stable than the holoprotein. However, in general the stability

of YkuN and YkuP to chaotropes appears quite similar to that observed other flavodoxins (e.g., refs *32* and *39*).

The *ykuN* and *ykuP* genes appear to be cotranscribed along with *ykuO* (a gene of unknown function, based on the identification of potential transcription signals on the nucleotide sequence: a vegetative σ^A RNA polymerase promoter sequence (5′-TTGACA-16nt-TTTAAA-3′) located 48 bp upstream of the ATG start codon of *ykuN* and a transcriptional termination sequence (5′-GGAACTGCTAAAACGGC-TGTTCCTTTTTTT) located 11 bp downstream of the TGA stop codon of *ykuP* (Figure 1). The adjacent *ykuQ* gene is likely to encode a tetrahydropicolinate *N*-acetyltransferase enzyme, which may participate in the biosynthesis pathways for *meso*-diaminopimelate and lysine (*52*). There are two potential Fur boxes (binding sites) overlapping the *ykuNOP* promoter region. In a recent paper dealing with gene expression in response to peroxide and superoxide stress, it was found that the *ykuNOP* genes are upregulated after addition of peroxide or paraquat (a superoxide generator) (*53*). This induction is most likely via Fur. Thus, in *B. subtilis* the two flavodoxin genes are expressed during iron limitation where one could expect a ferredoxin deficiency. The data reported here show that both YkuN and YkuP can support the hydroxylation activity of P450 BioI and one or both of these proteins could replace Fer (a Fe_4S_4 ferredoxin, which has been reported to support P450 BioI function, ref *17*) as an electron donor under conditions of iron limitation. Potentially, this affords the bacterial cell the capacity to ensure that the BioI reaction (required for biotin synthesis) can continue regardless of the levels of iron in the environment. Despite the observed structural differences between the flavodoxins, they both have similar potentiometric properties and both support the hydroxylation function of P450 BioI with similar efficiency. The reduction potentials of the YkuN or YkuP oxidized/semiquinone (E_1') and semiquinone/reduced (E_2') couples (−105/−105 mV and −382/−377 mV, respectively) show similar large separations between the couples as those seen for various other bacterial flavodoxins, including those from *E. coli* (FldA, $E_1' = -254$, $E_2' = -433$ mV), *D. vulgaris* ($E_1' = -143$, $E_2' = -435$ mV), and *C. beijerinckii* ($E_1' = -92$, $E_2' = -399$ mV) (*32*, *54*, *55*). In the fatty acid-bound form, the heme iron potential of P450 BioI is −199 mV, indicating that electron transfer from either YkuN or YkuP hydroquinone or semiquinone could be feasible but that electron transfer from the flavodoxin hydroquinone would be far more thermodynamically favorable.

Turnover studies using a FLDR, YkuN or YkuP, and P450 BioI system demonstrate the generation of hydroxylated products from a range of fatty acids. Other recent studies indicate that there is not a strong regioselectivity of monohydroxylation of myristic and palmitic acids by P450 BioI with monohydroxylation at a range of positions between ω-1 and ω-3 (myristic acid), and ω-1 and ω-5 (palmitic acid) on these substrates (*22*). Our studies extend the previous data regarding the flavodoxin-dependent hydroxylation of fatty acids, demonstrating that the P450 can oxygenate saturated and monounsaturated fatty acids of chain length varying between C_{12} and C_{16} and can perform two successive rounds of oxygenation in the case of the C_{16} substrates. Our own recent work on the *B. subtilis* CYP102A2 and CYP102A3 flavocytochromes P450 has shown that these enzymes mimic the better-characterized P450 BM3 system from *B. megaterium* and catalyze ω-1 to ω-3 hydroxylation of fatty acids (*56*). It is difficult to envisage that fatty acid oxygenation at these positions could be the physiologically relevant reaction of P450 BioI, given that reaction rates are severalfold slower than those catalyzed by the CYP102A2 or CYP102A3 enzymes. Thus, it appears that the hydroxylation activities observed with the isolated P450 BioI, YkuN or YkuP, and FLDR redox systems in vitro are unlikely to reflect the true in vivo role(s) of P450 BioI. Recent studies from De Voss's group have shown that very small amounts of pimelic acid (a known intermediate in the *B. subtilis* biotin synthesis pathway) can be synthesised by BioI and that this probably occurs through successive rounds of oxidative attack on the central carbons of long-chain fatty acids or fatty acyl CoA's. Specifically, oxygenation of a series of C_{14} substrates indicated that pimelic acid (albeit in very small amounts) could be produced most effectively using *R,R*- and *S,S*-7,8-dihydroxtetradecanoic acids (*57*). This appears to be consistent with P450 BioI catalyzing successive oxidations at central carbons on the lipid substrate, producing first alcohol and then diol, and finally catalyzing bond cleavage to generate monoacid and diacid products. A similar reaction scheme is known to occur for the cholesterol side chain cleavage enzyme P450scc (CYP11A1), which converts cholesterol to pregnenolone (*58*). Assuming that the envisaged reaction scheme for BioI is correct, then the hydroxylations observed close to the ω-terminus of fatty acids substrates will be competitive and inhibitory to the physiologically relevant reaction. To generate an efficient in vitro pimelic acid production system, the correct collection of component proteins will be required. It is thought that the host acyl carrier protein (ACP) loaded with lipid may be the true means of substrate delivery to P450 BioI (*21*) and may act to orientate P450 and substrate correctly for oxidation(s) at relevant bonds. The redox partner systems required to shuttle electrons from NAD(P)H to P450 BioI in vivo are likely to involve either or all (under different conditions) of Fer, YkuN, YkuP, and host flavodoxin/ferredoxin reductase(s). In ongoing work, we have cloned and expressed relevant *B. subtilis* partner proteins to reconstitute an efficient in vitro P450 BioI system that reproduces effectively the true activity of the natural cellular complex.

ACKNOWLEDGMENT

A.W.M. wishes to thank the Royal Society for the award of a Leverhulme Trust Senior Research Fellowship. The authors are also grateful to Professor Andrew Thomson at the University of East Anglia, Centre for Metalloprotein Spectroscopy and Biology, for access to facilities and helpful discussions.

REFERENCES

1. Coon, M. J. (2003) Multiple oxidants and multiple mechanisms in cytochrome P450 catalysis, *Biochem, Biophys. Res. Commun. 312*, 163−168.
2. Makris, T. M., Denisov, I. G., and Sligar, S. G. (2003) Haem-oxygen reactive intermediates: catalysis by the two-step, *Biochem. Soc. Trans. 31*, 516−519.
3. Sharma, P. K., De Visser, S. P., and Shaik, S. (2003) Can a single oxidant with two spin states masquerade as two different oxidants? A study of the sulfoxidation mechanism by cytochrome P450, *J. Am. Chem. Soc. 125*, 8698−8699.

4. Sevrioukova, I. F., Garcia, C., Li, H., Bhaskar, B., and Poulos, T. L. (2003) Crystal structure of putidaredoxin, the [2Fe-2S] component of the P450cam monooxygenase system from *Pseudomonas putida*, *J. Mol. Biol. 333*, 377−392.
5. Peterson, J. A., Lorence, M. C., and Amarneh, B. (1990) Putidaredoxin reductase and putidaredoxin. Cloning, sequence determination, and heterologous expression of the proteins, *J. Biol. Chem. 265*, 6066−6073.
6. Wang, M., Roberts, D. L., Paschke, R., Shea, T. M., Masters, B. S., and Kim, J. J. (1997) Three-dimensional structure of NADPH-cytochrome P450 reductase: prototype for FMN- and FAD-containing enzymes, *Proc. Natl. Acad. Sci. U.S.A. 94*, 8411−8416.
7. Hubbard, P. A., Shen, A. L., Paschke, R., Kasper, C. B., and Kim, J. J. (2001) NADPH-cytochrome P450 oxidoreductase. Structural basis for hydride and electron transfer, *J. Biol. Chem. 276*, 29163−29170.
8. Munro, A. W., Noble, M. A., Robledo, L., Daff, S. N., and Chapman, S. K. (2001) Determination of the redox properties of human NADPH-cytochrome P450 reductase, *Biochemistry 40*, 1956−1963.
9. Gutierrez, A., Paine, M., Wolf, C. R., Scrutton, N. S., and Roberts, G. C. K. (2002) Relaxation kinetics of cytochrome P450 reductase: internal electron transfer is limited by conformational change and regulated by coenzyme binding, *Biochemistry 41*, 4626−4637.
10. Narhi, L. O., Wen, L. P., and Fulco, A. J. (1988) Characterization of the protein expressed in *Escherichia coli* by a recombinant plasmid containing the *Bacillus megaterium* cytochrome P-450 BM-3 gene, *Mol. Cell. Biochem. 79*, 63−71.
11. Fulco, A. J. (1991) P450 BM-3 and other inducible bacterial P450 cytochromes: biochemistry and regulation, *Annu. Rev. Pharmacol. Toxicol. 31*, 177−203.
12. Munro, A. W., Leys, D., McLean, K. J., Marshall, K. R., Ost, T. W., Daff, S., Miles, C. S., Chapman, S. K., Lysek, D. A., Moser, C. C., Page, C. C., and Dutton, P. L. (2002) P450 BM3: the very model of a modern flavocytochrome, *Trends Biochem. Sci. 27*, 250−257.
13. Shimizu, H., Park, S., Lee, D., Shoun, H., and Shiro, Y. (2000) Crystal structures of cytochrome P450nor and its mutants (Ser286 to Val, Thr) in the ferric resting state at cryogenic temperature: a comparative analysis with monooxygenase cytochrome P450s, *J. Inorg. Biochem. 81*, 191−205.
14. Lee, D. S., Yamada, A., Sugimoto, H., Matsunaga, I., Ogura, H., Ichihara, K., Adachi, S., Park, S. Y., and Shiro, Y. (2003) Substrate recognition and molecular mechanism of fatty acid hydroxylation by cytochrome P450 from *Bacillus subtilis*. Crystallographic, spectroscopic, and mutational studies, *J. Biol. Chem. 278*, 9761−9767.
15. Roberts, G. A., Grogan, G., Greter, A., Flitsch, S. L., and Turner, N. J. (2002) Identification of a new class of cytochrome P450 from a *Rhodococcus* sp, *J. Bacteriol. 184*, 3898−3908.
16. Green, A. J., Rivers, S. L., Cheesman, M. R., Reid, G. A., Quaroni, L. G., Macdonald, I. D. G., Chapman, S. K., and Munro, A. W. (2001) Expression, purification and characterization of cytochrome P450 BioI: a novel P450 involved in biotin synthesis in *Bacillus subtilis*, *J. Biol. Inorg. Chem. 6*, 523−533.
17. Green, A. J., Munro, A. W., Cheesman, M. R., Reid, G. A., von Wachenfeldt, C., and Chapman, S. K. (2003) Expression, purification and characterisation of a *Bacillus subtilis* ferredoxin: a potential electron transfer donor to cytochrome P450 BioI. *J. Inorg. Biochem. 93*, 92−99.
18. Schiffler, B., Kiefer, M., Wilken, A., Hannemann, F., Adolph, H. W., and Bernhardt, R. (2001) The interaction of bovine adrenodoxin with CYP11A1 (cytochrome P450scc) and CYP11B1 (cytochrome P45011β). Acceleration of reduction and substrate conversion by site-directed mutagenesis of adrenodoxin, *J. Biol. Chem. 276*, 36225−36232.
19. Poupin, P., Ducrocq, V., Hallier-Soulier, S., and Truffaut, N. (1999) Cloning and characterization of the genes encoding a cytochrome P450 (PipA) involved in piperidine and pyrrolidine utilization and its regulatory protein (PipR) in *Mycobacterium smegmatis* mc2155, *J. Bacteriol. 181*, 3419−3426.
20. Kunst, K., Ogasawara, N., Moszer, I., Albertini, A. M., Azevedo, V., et al. (1997) The complete genome sequence of the Gram-positive bacterium *Bacillus subtilis*, *Nature 390*, 249−256.
21. Stok, J. E., and De Voss, J. (2000) Expression, purification, and characterization of BioI: a carbon−carbon bond cleaving cytochrome P450 involved in biotin biosynthesis in *Bacillus subtilis*, *Arch. Biochem. Biophys. 384*, 351−360.
22. Cryle, M. J., Matovic, N. J., and De Voss, J. J. (2003) Products of cytochrome P450 BioI (CYP107H1)-catalyzed oxidation of fatty acids, *Org. Lett. 5*, 3341−334.
23. Hawkes, D. B., Adams, G. W., Burlingame, A. L., Ortiz de Montellano, P. R., and De Voss, J. J. (2002) Cytochrome $P450_{cin}$ (CYP176A), isolation, expression, and characterization, *J. Biol. Chem. 277*, 27725−27732.
24. Zhao, Q., Modi, S., Smith, G., Paine, M., McDonagh, P. D., Wolf, C. R., Tew, D., Lian, L.-Y., Roberts, G. C. K., and Driessen, H. P. (1999) Crystal structure of the FMN-binding domain of human cytochrome P450 reductase at 1.93 Å resolution, *Protein Sci. 8*, 298−306.
25. Mayhew, S. G., and Tollin, G. (1992) General properties of flavodoxins, in *Chemistry and Biochemistry of Flavoenzymes* (Müller, F., Ed.), Vol. III, pp 389−426, CRC Press, Boca Raton, FL.
26. Fujii, K., Galivan, J. H., and Hennekens, F. M. (1977) Activation of methionine synthase: A further characterization of the flavoprotein system, *Arch. Biochem. Biophys. 178*, 662−670.
27. Nieva-Gomez, D., Roberts, G. P., Klevickis, S., and Brill, W. J. (1980) Electron transport to nitrogenase in *Klebsiella pneumoniae*. *Proc. Natl. Acad. Sci. U.S.A. 77*, 2255−2258.
28. Blaschkowski, H. P., Neuer, G., Ludwig-Festl, M., and Knappe, J. (1982) Routes of flavodoxin and ferredoxin reduction in *Escherichia coli*. CoA-acylating pyruvate:flavodoxin and NADPH: flavodoxin oxidoreductases participating in the activation of pyruvate-formate lyase, *Eur. J. Biochem. 123*, 563−569.
29. Berkovitch, F., Nicolet, Y., Wan, J. T., Jarrett, J. T., and Drennan, C. L. (2004) Crystal structure of biotin synthase, an S-adenosylmethionine-dependent radical enzyme, *Science 303*, 76−79.
30. Ludwig, M., and Luschinsky, C. L. (1992) Structure and redox properties of clostridial flavodoxin, in *Chemistry and Biochemistry of Flavoenzymes* (Müller, F., Ed.) Vol. III, pp 427−466, CRC Press, Boca Raton, FL.
31. Baichoo, N., Wang, T., Ye, R., and Helmann, J. D. (2002) Global analysis of the *Bacillus subtilus* Fur regulon and the iron starvation stimulon, *Mol. Microbiol. 45*, 1613−1629.
32. McIver, L., Leadbeater, C., Campopiano, D. J., Baxter, R. L., Daff, S. N., Chapman, S. K., and Munro, AW. (1998) Characterisation of flavodoxin $NADP^+$ oxidoreductase and flavodoxin; key components of electron transfer in *Escherichia coli*, *Eur. J. Biochem. 257*, 577−585.
33. Birch, O. M., Fuhrmann, M., and Shaw, N. M. (1995) Biotin synthase from *Escherichia coli*, an investigation of the low molecular weight and protein components required for activity *in vitro*, *J. Biol. Chem. 270*, 19158−19165.
34. Sambrook, J., Fritsch, E. F., and Maniatis, T. (1989) *Molecular Cloning: A Laboratory Manual*, 2nd ed., Cold Spring Harbor Laboratory Press, Cold Spring Harbor, NY.
35. Sanger, F., Nicklen, S., and Coulson, A. R. (1977) DNA sequencing with chain-terminating inhibitors, *Proc. Natl. Acad. Sci. U.S.A. 74*, 5463−5467.
36. Lawson, R. J., Leys, D., Sutcliffe, M. J., Kemp, C. A., Cheesman, M. R., Smith, S. J., Clarkson, J., Smith, W. E., Haq, I., Perkins, J. B., and Munro, A. W. (2004) Thermodynamic and biophysical characterization of cytochrome P450 BioI from *Bacillus subtilis*, *Biochemistry 43*, 12410−12426.
37. Macheroux P., Massey V., Thiele D. J., and Volokita M. (1991) Expression of spinach glycolate oxidase in *Saccharomyces cerevisiae*: purification and characterization, *Biochemistry 30*, 4612−4619.
38. Wassink, J. H., and Mayhew, S. G. (1975) Fluorescence titration with apoflavodoxin: a sensitive assay for riboflavin 5′-phosphate and flavin adenine dinucleotide in mixtures, *Anal. Biochem. 68*, 609−616.
39. Apiyo, D., Guidty, J., and Wittung-Stafshede, P. (2000) No cofactor effect on equilibrium unfolding of *Desulfovibrio desulfuricans* flavodoxin, *Biochim. Biophys. Acta 1479*, 214−224.
40. Pueyo, J. J., Curley, G. P., and Mayhew, S. G. (1996) Kinetics and thermodynamics of the binding of riboflavin, riboflavin 5′-phosphate and riboflavin 3′, 5′-bisphosphate by apoflavodoxins, *Biochem. J. 313*, 855−861.
41. Daff, S. N., Chapman, S. K., Turner, K. L., Holt, R. A., Govindaraj, S., Poulos, T. L., and Munro, A. W. (1997) Redox control of the catalytic cycle of flavocytochrome P-450 BM3, *Biochemistry 36*, 13816−13823.
42. Dutton, P. L. (1978) Redox potentiometry: determination of midpoint potentials of oxidation−reduction components of biological electron-transfer systems, *Methods Enzymol. 54*, 411−435.

43. Hoover, D. M., and Ludwig, M. L. (1997) A flavodoxin that is required for enzyme activation: The structure of oxidized flavodoxin from *Escherichia coli* at 1.8 Å resolution, *Protein Sci. 6*, 2525−2537.
44. Noble, M. A., Munro, A. W., Rivers, S. L., Robledo, L., Daff, S. N., Yellowlees, L. J., Shimizu, T., Sagami, I., Guillemette, J. G., and Chapman S. K. (1999) Potentiometric analysis of the flavin cofactors of neuronal nitric oxide synthase, *Biochemistry 38*, 16413−16418.
45. Arnold Murray, T., and Swenson, R. P. (2003) Mechanism of flavin mononucleotide cofactor binding to the *Desulfovibrio vulgaris* flavodoxin. 1. Kinetic evidence for cooperative effects associated with the binding of inorganic phosphate and the 5′-phosphate moiety of the cofactor, *Biochemistry 42*, 2307−2316.
46. Chang, F.-C., and Swenson, R. P. (1999) The midpoint potential for the oxidized-semiquinone couple for Gly57 mutants of the *Clostridium beijerinkii* flavodoxin correlate with changes in the hydrogen-bonding interaction with the proton on N5 of the reduced flavin mononucleotide cofactor as measured by NMR chemical shift temperature dependencies, *Biochemistry 38*, 7168−7176.
47. Walsh, M. A., McCarthy, A., O'Farrell, P. A., McArdle, P., Cunningham, D. D., Mayhew, S. G., and Higgins, T. M. (1998) X-ray crystal structure of the *Desulfovibrio vulgaris* (Hildenborough) apoflavodoxin-riboflavin complex, *Eur. J. Biochem. 258*, 362−371.
48. Mayhew, S. G. (1971) Studies on flavin binding in flavodoxins, *Biochim. Biophys. Acta 235*, 289−302.
49. Curley, G. P., Carr, M. C., Mayhew, S. G., and Voordouw, G. (1991) Redox and flavin-binding properties of recombinant flavodoxin from *Desulfovibrio vulgaris* (Hildenborough), *Eur. J. Biochem. 202*, 1091−1100.
50. Nuallain, B. O., and Mayhew, S. G. (2002) A comparison of the urea-induced unfolding of apoflavodoxin and flavodoxin from *Desulfovibrio vulgaris*, *Eur. J. Biochem. 269*, 212−223.
51. Hintz, J. M., Mock, D. M., Peterson, L. L., Tuttle, K., and Peterson, J. A. (1982) Equilibrium and kinetic studies of the interaction of cytochrome P-450cam and putidaredoxin, *J. Biol. Chem. 257*, 14324−14332.
52. Beaman, T. W., Vogel, K. W., Drueckhammer, D. G., Blanchard, J. S., and Roderick, S. L. (2002) Acyl group specificity at the active site of tetrahydridipicolinate N-succinyltransferase, *Protein Sci. 11*, 974−979.
53. Mostertz, J., Scharf, C., Hecker, M., and Homuth, G. (2004) Transcriptome and proteome analysis of *Bacillus subtilis* gene expression in response to superoxide and peroxide stress, *Microbiology 150*, 497−512.
54. McCarthy, A. A., Walsh, M. A., Verma, C. S., O'Connell, D. P., Reinhold, M., Yalloway, G. N., D'Arcy, D., Higgins, T. M., Voordouw, G., and Mayhew, S. G. (2002) Crystallographic investigation of the role of aspartate 95 in the modulation of the redox potentials of *Desulfovibrio vulgaris* flavodoxin, *Biochemistry 41*, 10950−10962.
55. Mayhew, S. G. (1971) Properties of two clostridial flavodoxins, *Biochim. Biophys. Acta 235*, 276−288.
56. Truan, G., Komandla, M. R., Falck, J. R., and Peterson, J. A. (1999) P450 BM3: absolute configuration of the primary metabolites of palmitic acid, *Arch. Biochem. Biophys. 366*, 192−198.
57. Cryle, M. J., and De Voss, J. J. (2004) Carbon−carbon bond cleavage by cytochrome P450 BioI (CYP107H1), *Chem. Commun. 86*, 86−87.
58. Lambeth, J. D., Kitchen, S. E., Farooqui, A. A., Tuckey, R., and Kamin, H. (1982) Cytochrome $P450_{scc}$-substrate interactions: Studies of binding and catalytic activity using hydroxycholesterols, *J. Biol. Chem. 257*, 1876−1884.
59. Edmondson, D. E., and Tollin, G. (1971) Flavoprotein chemistry. I. Circular dichroism studies of the flavin chromophore and the relation between redox properties and flavin environment in oxidases and dehydrogenases, *Biochemistry 10*, 113−124.

BI049131T